CHAPTER 9

OPTIMAL LARGE - ANGLE SINGLE - AXIS MANEUVERS OF FLEXIBLE SPACECRAFT

9.1 INTRODUCTION

In this chapter, and in the one following, we consider the problem of maneuvering a flexible vehicle through large rigid body rotations about a principal axis, while minimizing the structural deformations during the maneuver. The vehicle is assumed to have several discrete control actuators which act at various points on the structure. We consider both linear and nonlinear maneuver cases and the associated numerical methods required for solving them. Several general types of terminal maneuver boundary conditions are considered for the rigid body motion; however, in all the maneuvers considered we impose the constraint of zero structural deformations and deformation rates at the terminal maneuver time.

The motion of the class of vehicles under consideration is described by a system of hybrid coordinates (see Chapter 5). The coordinates are referred to as hybrid, because the equations of motion are defined by a coupled set of ordinary and partial differential equations. The ordinary differential equations govern the discrete coordinates for modeling the rotations and translations of rigid bodies, whereas the partial differential equations govern the distributed coordinates for modeling the deformations of elastic members.

The procedure most widely used for analyzing such hybrid systems is a spatial discretization (see Chapter 5), whereby the partial differential equations are converted into infinite sets of ordinary differential equations. However, we assume throughout Chapters 9 and 10 that the infinite sets of ordinary differential equations have been suitably approximated by a finite (truncated) set. The theoretical issues associated with truncation and control spillover effects (i.e. excitation of unmodeled modes) are not dealt with formally here. Nevertheless, it is possible to develop ad hoc techniques

for specifying the modes to be retained in the dynamical model and making assessments of spillover effects via simulation studies. However, the model errors (due to a poor model definition or inaccurate specification of model parameter values) remains a most serious and unresolved problem. Salvation from ever present model errors most probably lies in augmenting the open-loop controls (of the present discussion) by robust feedback controls.

One popular spatial discretization procedure [refs. 1,2] can be carried out using a Ritz approach, whereby the deformations of the continuous elastic members are represented by a finite series of known (admissible) space-dependent functions multiplied by time-dependent generalized coordinates. Alternatively, we can use a general-purpose finite element method to discretize the mathematical model (see Chapter 5).

For the specific configuration considered in this chapter and the following chapter (see Fig. 9.1), the vehicle consists of a rigid hub with four identical, cantilevered elastic appendages attached symmetrically about the central hub. In particular, we consider the following idealizations: (i) single-axis maneuvers; (ii) in-plane motion; (iii) anti-symmetric deformations; (iv) small linear flexural deformations; and (v) the control actuators are modeled as massless concentrated torque generating devices. The control system for the vehicle is taken to consist of: (i) a single torque actuator acting upon the rigid part of the structure; and (ii) each elastic appendage is assumed to have a single torque actuator acting upon the appendage at mid-span. The extension to the case of multiple torquers along each appendage is straightforward; however only the mid-span appendage actuator case is considered in the present chapter.

The necessary conditions for the optimal single-axis maneuver are presented in two parts. The first part (Sections 9.2-9.4) consists of the formulation and solution of the linear time-invariant problem. The second part

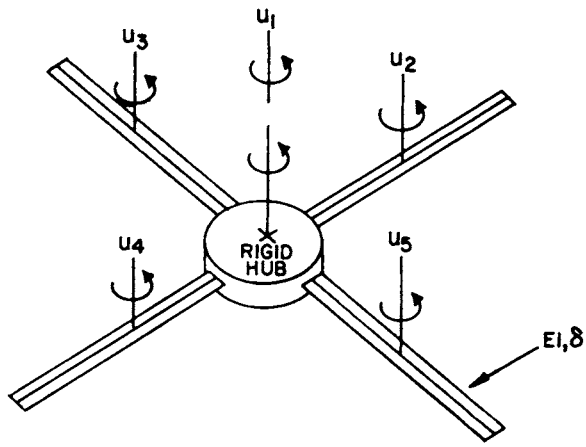

Figure 9.1 Undeformed Structure

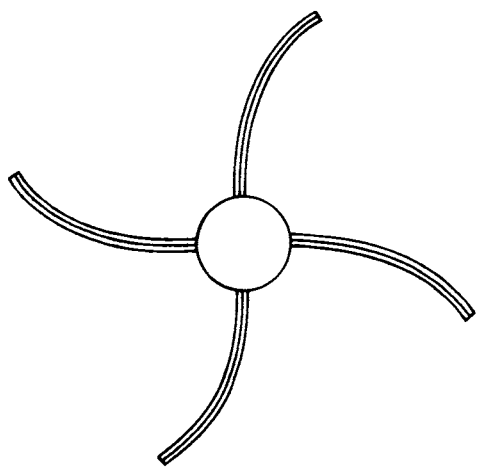

Figure 9.2 Antisymmetric Deformation

(Section 9.5.1) consists of presenting the nonlinear equations which include the rotational stiffening effect. In Section 9.5.2 a differential equation continuation method is presented for solving the nonlinear TPBVP; this method makes efficient use of the solution for the initial co-states obtained from the linear time-invariant problem. In Section 9.6, we provide numerical results which demonstrate the validity and utility of the formulations described herein.

9.2 EQUATIONS OF MOTION

For the vehicle depicted in Figure 9.1, the equations of motion can be obtained from Hamilton's extended principle (see Chapter 5).

$$\int_{t_1}^{t_2} (\delta L + \delta W)dt = 0 \tag{9.1}$$

subject to

$$\delta\theta = \delta u = 0 \text{ at } t_1, t_2$$

where $L = T - V$ is the system Lagrangian, δW represents the virtual work, $\delta\theta$ represents a virtual rotation, and δu represents a virtual elastic displacement.

The kinetic and potential energy expressions for the vehicle can be shown to be (see Sections 5.3.2 and 5.3.3)

$$T = \frac{1}{2}\dot{\theta}^2[\hat{I} + 4\int_r^{r+L}(u^2 - p^2)dm] + 2\int_r^{r+L}\dot{u}^2dm + 4\dot{\theta}\int_r^{r+L}x\dot{u}dm \tag{9.2a}$$

$$V = 2\int_r^{r+L} EI[\frac{\partial^2 u}{\partial x^2}]^2dx \tag{9.2b}$$

with

$$p^2 = \frac{1}{2}[(r+L)^2 - r^2 - x^2](\frac{\partial u}{\partial x})^2, \tag{9.3}$$

where $\hat{I}$ denotes the moment of inertia of the undeformed vehicle about the axis of rotation, r denotes the radius of the rigid hub, L denotes the undeformed length of the elastic appendages, $p^2 \neq 0$ accounts for the constraint that there

is no local stretching of the deforming appendages, and EI denotes the flexural rigidity of the appendages.

The virtual work in this example is

$$\delta W = \sum_{k=1}^{N} Q_k \delta q_k \tag{9.4}$$

where the generalized forces Q_k can be shown to be (see Section 5.3.1)

$$Q_k = \mathbf{f} \cdot \frac{\partial \dot{\mathbf{R}}}{\partial \dot{q}_k} + \frac{\partial \boldsymbol{\omega}}{\partial \dot{q}_k} \cdot \left[\int_v \mathbf{r} \times d\mathbf{f} + \int_v \mathbf{u} \times d\mathbf{f}\right] + \int_v \frac{\partial \overset{\circ}{\mathbf{u}}}{\partial \dot{q}_k} \cdot d\mathbf{f} \tag{9.5}$$

where $\overset{\circ}{\mathbf{u}} \equiv \frac{d}{dt}(\mathbf{u})_B$, B denotes a frame fixed in the rigid hub, $\dot{q}_k(t)$ denotes the time derivative of the kth generalized coordinate, and

$$\mathbf{f} = \int_v d\mathbf{f} \tag{9.6}$$

Before applying Hamilton's extended principle, we express (by the "assumed modes" method of Section 5.4.1 and refs. 1,2) the elastic displacements as the following series:

$$\mathbf{u}(x,t) = u(x,t)\hat{\mathbf{b}}_2 \ , \ u(x,t) = \sum_{k=1}^{n} \eta_k(t)\phi_k(x - r) \tag{9.7}$$

where $\eta_k(t)$ denotes the kth generalized coordinate, $\phi_k(x - r)$ denotes the kth assumed admissible mode shape, and n denotes the number of terms retained in the approximation.

On introducing Eq. 9.7 into Eqs. 9.2 and 9.3, we obtain the system Lagrangian

$$L = \frac{\hat{I}}{2}\dot{\theta}^2 + \frac{1}{2}\dot{\eta}^T M_{\eta\eta}\dot{\eta} + \dot{\theta}\dot{\eta}^T \mathbf{M}_{\theta\eta} - \frac{1}{2}\dot{\theta}^2 \eta^T[\Xi - \mathbf{M}_{\eta\eta}]\eta - \frac{1}{2}\eta^T K_{\eta\eta}\eta \tag{9.8}$$

where

$$\eta = [\eta_1, \eta_2, \ldots, \eta_n]^T$$

$$[M_{\eta\eta}]_{kp} = 4\int_r^{r+L} \phi_k(x - r)\phi_p(x - r)dm \ , \quad (n \times n)$$

$$[M_{\theta\eta}]_k = r\int_r^{r+L} x\,\phi_k(x-r)dm \quad , \quad (n \times 1)$$

$$[\Xi]_{kp} = 4\int_r^{r+L} \frac{1}{2}\left[(r+L)^2 - r^2 - x^2\right]\phi_k'(x-r)\phi_p'(x-r)dm \quad , \quad (n \times n)$$

$$[K_{\eta\eta}]_{kp} = 4\int_r^{r+L} EI\phi_k''(x-r)\phi_p''(x-r)dx \quad , \quad (n \times n)$$

$$(\,)' \equiv \frac{d}{dx}(\,) \quad , \quad (\,)'' \equiv \frac{d^2}{dx^2}(\,)$$

On introducing Eq. 9.7 into Eq. 9.5 we find for Q_k

$$Q_1 = u_1 + 4u_2 \qquad \text{(rigid body torque)} \tag{9.9}$$

$$Q_{k+1} = 4\phi_k'(x_p - r)u_2 \qquad \text{(elastic appendage torque)} \tag{9.10}$$

where x_p is the coordinate locating the point of application of the control torque on the elastic appendage. Equations 9.9 and 9.10 are obtained by replacing the concentrated control torques by equivalent force pairs (couples) using spatial delta functions to locate the points of application ($x = x_p \pm r_c$) of the couple forces, where the lever arm of the couple is denoted by r_c and the couple forces are denoted by $\pm F_c$. The concentrated torque of strength u_2 is formed by letting r_c approach zero while F_c becomes infinite in such a manner that twice the product of F_c and r_c approaches the limit u_2:

$$\lim_{F \to \infty, r_c \to 0} (2r_c F_c) = u_2$$

The derivative of the mode shape arises in Eq. 9.10 as a result of the limit process that produces u_2.

Substituting Eqs. 9.7, 9.8, 9.9a and 9.10 into Eq. 9.1 yields Lagrange's equations

$$\frac{d}{dt}\left(\frac{\partial L}{\partial \dot{\theta}}\right) - \frac{\partial L}{\partial \theta} = u_1 + 4u_2 \tag{9.11}$$

$$\frac{d}{dt}\left(\frac{\partial L}{\partial \dot{\eta}}\right) - \frac{\partial L}{\partial \eta} = F\,u_2 \tag{9.12}$$

where

$$F = 4[\phi_1'(x_p - r)\ ,\ \phi_2'(x_p - r), \ldots, \phi_n'(x_p - r)]^T.$$

The equations of motion follow as:

$$(\hat{I} - \eta^T m^* \eta)\ddot{\theta} + M_{\theta\eta}^T \ddot{\eta} - 2\dot{\theta}\dot{\eta}^T m^* \eta = u_1 + 4u_2 \tag{9.13}$$

$$M_{\theta\eta}\ddot{\theta} + M_{\eta\eta}\ddot{\eta} + [K_{\eta\eta} + \dot{\theta}^2 m^*]\eta = Fu_2 \tag{9.14}$$

where $m^* = \Xi - M_{\eta\eta}$.

9.3 STATE SPACE FORMULATION

The desired state space form of Eqs. 9.13 and 9.14 for the linear time-invariant problem is obtained upon invoking the following two assumptions: First, the small deflection assumption (due to the linear stress-strain assumption underlying Eq. 9.2) permits the quadratic deflection terms in Eqs. 9.13 and 9.14 to be dropped. Second, since the continuation method for the nonlinear problem (Section 9.5.2) requires the solution for the linear solution as the starting iterative, the $\dot{\theta}^2$ term (i.e., the rotational stiffening effect) is for the present deleted. Subject to the above assumptions, Eqs. 9.13 and 9.14 can be cast in the familiar linear matrix form

$$M\ddot{\xi} + K\xi = Pu \tag{9.15}$$

where the *configuration vector* $\xi(t)$, the *control vector* $u(t)$, and the constant coefficient matrices are

$$\xi = \begin{Bmatrix} \theta \\ \eta \end{Bmatrix} \; ; \; M = \begin{bmatrix} \hat{I} & M_{\theta\eta}^T \\ M_{\theta\eta} & M_{\eta\eta} \end{bmatrix} \; ; \; K = \begin{bmatrix} 0 & 0^T \\ 0 & K_{\eta\eta} \end{bmatrix} \tag{9.16}$$

$$P = \begin{bmatrix} 1 & 4 \\ 0 & F \end{bmatrix} \; ; \; u = \begin{Bmatrix} u_1 \\ u_2 \end{Bmatrix}$$

and $M = M^T > 0$, $K = K^T \geq 0$.

Equation 9.15 can be written in uncoupled form by introducing the coordinate transformation from configuration position and velocity (ξ, $\dot{\xi}$) to modal displacement and velocity (s_1,s_2), as follows:

$$\xi = Es_1; \quad \dot{\xi} = E\dot{s}_1 \equiv Es_2; \quad s_2 \equiv \dot{s}_1 \tag{9.17}$$

where E is the matrix of normalized eigenvectors for the generalized eigenvalue problem

$$\lambda_r^2 M e_r = K e_r \tag{9.18}$$

where λ_r^2 is the rth eigenvalue, e_r is the rth eigenvector, and $E = [e_1 \ e_2 \ \ldots \ e_N]$ has been normalized subject to

$$E^T M E = I, \tag{9.19}$$

from which it follows that

$$E^T K E \equiv [\Delta] = \text{Diag.}\ (\lambda_1^2, \ldots, \lambda_N^2) \ ; \ (N = n + 1) \tag{9.20}$$

On introducing Eq. 9.17 into Eq. 9.15 and premultiplying the resulting equation by E^T the modal space equation of motion follows as

$$\ddot{s}_1 + [\Delta] s_1 = D u \ ; \ D = E^T P \tag{9.21}$$

or

$$\dot{s} = A s + B u \tag{9.22}$$

where

$$A = \begin{bmatrix} 0 & I \\ -\Delta & 0 \end{bmatrix} \ , \quad B = \begin{bmatrix} 0 \\ D \end{bmatrix} \ , \quad s = \begin{Bmatrix} s_1 \\ s_2 \end{Bmatrix} \tag{9.23}$$

9.4 OPTIMAL CONTROL PROBLEM

9.4.1 Statement of the Problem

We consider here the rotational dynamics of a flexible space vehicle restricted to a single-axis large-angle maneuver about a principal axis, where the system dynamics is governed by Eq. 9.22. In particular, we seek a solution of Eq. 9.22 satisfying the prescribed terminal states

$$\xi_o = [\theta_o, \ \eta(t_o)]^T \ , \quad \dot{\xi}_o = [\dot{\theta}_o, \ \dot{\eta}(t_o)]^T \tag{9.24a}$$

and

$$\xi_f = [\theta_f, \ \eta(t_f)]^T \ , \quad \dot{\xi}_f = [\dot{\theta}_f, \ \dot{\eta}(t_f)]^T \tag{9.24b}$$

where we impose the constraint that $\eta(t_f) = \dot{\eta}(t_f) = 0$ on the right-hand side of Eq. 9.24b at the final time. We also seek the torque history $u(t)$ which generates an optimal solution of Eq. 9.22, initiating at Eq. 9.24a and

terminating at Eq. 9.24b which minimizes the performance index

$$J = \frac{1}{2}\int_{t_o}^{t_f} [u^T W_{uu} u + s^T W_{ss} s]dt \qquad (9.25)$$

where $W_{uu} = W_{uu}^T > 0$ is a weight matrix for the control and $W_{ss} = W_{ss}^T \geq 0$ is a weight matrix for the state. If W_{ss} and W_{uu} are selected to have a block diagonal structure, our performance index can be interpreted as seeking to minimize a functional which is proportional to a summation of positive measures of (i) control effort, (ii) kinetic energy, and (iii) elastic potential energy. Although the selection of Eq. 9.28 has been made for convenience, it is recognized that many other reasonable performance indices are possible (e.g., see refs. [3-7]). Based on our own numerical experience, we have found that the numerical values selected for W_{uu} and W_{ss} in Eq. 9.25 should be adjusted experimentally according to: (i) how many elastic modes are retained in Eq. 9.7; and (ii) the numerical values of the weights have been found to be restricted to particular ranges in order to ensure that the resulting solutions are numerically stable and (iii) the controlled response is qualitatively "desirable" with all state and control variables moving within physically admissible bounds. For the case of feedback control, these weight matrices can be chosen to optimize the placement and sensitivity of the closed loop eigenvalues as is discussed in Section 6.7.3. The particular weighting scheme used is discussed in Section 9.6.

9.4.2 Derivation of Necessary Conditions from Pontryagin's Principle

In preparing to make use of Pontryagin's necessary conditions, we introduce the Hamiltonian functional

$$H = \frac{1}{2}(u^T W_{uu} u + s^T W_{ss} s) + \lambda^T(As + Bu) \qquad (9.26)$$

where the λ's are Lagrange multipliers (also known as *co-state* or *adjoint* variables). Pontryagin's principle (Chapter 6) requires as necessary conditions that the λ's satisfy co-state differential equations derivable from

the gradient of H as

$$\dot{\lambda} = -\frac{\partial H}{\partial \mathbf{s}} = -[W_{ss}\mathbf{s} + A^T\lambda] \tag{9.27}$$

and that the control torque $\mathbf{u}(t)$ must be chosen at every instant so that the Hamiltonian of Eq. 9.26 is minimized. That is, for $\mathbf{u}(t)$ continuous and unbounded, we require

$$\frac{\partial H}{\partial \mathbf{u}} = \mathbf{0} = W_{uu}\mathbf{u} + B^T\lambda, \tag{9.28}$$

and $\frac{\partial^2 H}{\partial \mathbf{u}^2} = W_{uu} > 0$ from which the optimal torque is determined as

$$\mathbf{u} = -W_{uu}^{-1}B^T\lambda \tag{9.29}$$

The state and co-state differential equations are summarized as:

State Equations

$$\dot{\mathbf{s}} = A\mathbf{s} - BW_{uu}^{-1}B^T\lambda \tag{9.30a}$$

Co-state Equations

$$\dot{\lambda} = -W_{ss}\mathbf{s} - A^T\lambda \tag{9.30b}$$

9.4.3 Solution for the Initial Co-States

We observe in Eq. 9.30 that the boundary conditions for $\mathbf{s}(t)$ are known both initially and finally, whereas all boundary conditions for $\lambda(t)$ are unknown. Thus, application of Pontryagin's principle has led, as usual, to a TPBVP. To obtain the solution for Eq. 9.30, we first introduce the merged state vector

$$\mathbf{x}(t) = [\mathbf{s}(t), \lambda(t)]^T \tag{9.31}$$

so that the state and co-state differential equations can be cast in the first-order form:

$$\dot{\mathbf{x}}(t) = \Omega\mathbf{x}(t) \tag{9.32}$$

where the constant coefficient matrix is

$$\Omega = \begin{bmatrix} A & -BW_{uu}^{-1}B^T \\ -W_{ss} & -A^T \end{bmatrix}$$

Since Ω is constant, it is well known that Eq. (9.32) possesses the solution

$$x(t) = e^{\Omega(t-t_o)} x(t_o) \tag{9.33}$$

where $e^{\Omega t}$ is the 4N by 4N exponential matrix.

The exponential matrix can be calculated by any one of a variety methods described by Moler and Loan [ref. 8] or by Ward [ref. 9]. We have found particularly useful the diagonal Pade´ approximation approach [ref. 9] used in conjunction with the identity

$$e^{\Omega t} = (e^{\Omega t/2^n})^{2^n} \tag{9.34}$$

where n is the smallest integer such that the max. $\|\Omega t\|/2^n \leq 1$, and $\|(..)\|$ denotes a suitable matrix norm (we often use $\|Q\| = \text{Max}|Q_{ij}|$, the largest element of $Q = \Omega(t_f - t_o)$).

Having computed $\phi(t,t_o) \equiv e^{\Omega(t-t_o)}$, Eq. 9.33 can be evaluated at the final time and cast in the partitioned form

$$\begin{Bmatrix} s(t_f) \\ \lambda(t_f) \end{Bmatrix} = \begin{bmatrix} \phi_{ss} & \phi_{s\lambda} \\ \phi_{\lambda s} & \phi_{\lambda\lambda} \end{bmatrix} \begin{Bmatrix} s(t_o) \\ \lambda(t_o) \end{Bmatrix} \tag{9.35}$$

Upon carrying out the partitioned matrix multiplication in Eq. 9.35 for $s(t_f)$, we find

$$s(t_f) = \phi_{ss} s(t_o) + \phi_{s\lambda} \lambda(t_o) \tag{9.36}$$

Since $s(t_o)$ and $s(t_f)$ are known above, the solution for the unknown $\lambda(t_o)$ follows from

$$\phi_{s\lambda} \lambda(t_o) = s(t_f) - \phi_{ss} s(t_o) \tag{9.37}$$

where Eq. 9.37 is linear in $\lambda(t_o)$, and the solution for $\lambda(t_o)$ is easily obtained using Gaussian elimination, Cholesky decomposition or some other linear equation solution method. The time histories for the state and co-state are recursively generated at discrete times by the following difference equation:

$$x_{k+1} = e^{\Omega \Delta t} x_k \quad , \quad x_o = x(t_o) \quad , \quad k = 0, \ldots, N-1 \tag{9.38}$$

where x_k denotes the merged state at time $t_k = k\Delta t + t_o$, $\Delta t = (t_f - t_o)/N$,

and N is an integer that specifies the number of discrete times at which the solution for $x(t)$ is required. However, there are two potential stumbling blocks which can thwart the solution process outlined above. First, if $\Phi_{s\lambda}$ is nearly singular, then the solution for $\lambda(t_o)$ is poorly determined. Second, in some cases, an accurate solution for the matrix exponential cannot be calculated (depending, in a complicated way, upon Ω).

Most commonly, when numerical difficulties are encountered in the solution for $\lambda(t_o)$, the root cause is due to the differential equations of Eq. 9.32 being "stiff"; in the sense that some solutions increase and others decrease rapidly as the independent variable changes. If such numerical difficulties are encountered, there are several courses of action one can take to overcome the stiff behavior of Eq. 9.32: (i) use a shorter maneuver time interval ($t_f - t_o$); (ii) redefine the problem in order to compress the eigenvalue spectrum of Ω (e.g. select new control and state weighting matrices); (iii) introduce the intermediate times $t_o < t_1 < t_2 < \ldots < t_f$, in order to convert the two-point boundary-value problem into a multi-point boundary-value problem so as to limit the growth of $e^{\Omega(t_k - t_{k-1})}$ in the kth sub-interval. We present here only cases in which direct application of the solution process above leads to an accurate $\lambda(t_o)$, or remedial actions (i) or (ii) have already been taken to restructure the intially defined problem.

9.4.4 Free Final Angle Transversality Conditions

We consider here the problem of a maneuvering spacecraft where the final angle achieved at the end of the maneuver is determined as part of the solution process. This class of attitude maneuvers (where the free final angle boundary condition is appropriate) usually embodies those maneuvers for which the final angular rate is specified, and the final maneuver angle is not of interest (this problem has also been considered in Chapter 6, for rigid body spacecraft maneuvers).

There are principally three reasons why we consider the free final angle maneuver problem. First, in seeking to minimize a performance index we must recognize that the index, J, may vary significantly as a function of the specified final angle, θ_f. Consequently, by allowing θ_f to go "free" and imposing the corresponding transversality condition, we recover the particular angle $\theta_f = \theta_f^*$ which minimizes $J(\theta_f)$. Second, for the example maneuvers discussed in Chapter 7 and in Section 9.6, it is demonstrated that the so-called spin reversal phenomena, which occurs in many fixed-final time and fixed-final angle maneuvers, disappears when the final angle (or the final time) is left "free", to be determined by the transversality condition. Third, when the free final angle transversality condition selects the *natural boundary condition* for the final rigid body maneuver angle, we find that the peak torque requirements and associated structural deformations in the vehicle are usually minimized.

Before we proceed with determining the necessary transversality conditions for the free final angle maneuvers, we recall that the transversality conditions (see Section 6.2) are derived most naturally in terms of configuration space state variables, whereas in this chapter the optimal control problem has been formulated in terms of modal space state variables. Hence, a transformation is required in order to relate the required state, co-state, and associated state transition matrix in terms of either configuration space or modal space variables.

Since the solution in terms of modal space variables is available from Section 9.4.3, the first order of business is to map the modal space state transition matrix of Eq. 9.33, repeated here as

$$\phi(t,t_o) = e^{\Omega(t-t_o)} \tag{9.39}$$

into its corresponding configuration space form. In order to appreciate the structure of the transformation matrix, we first recognize that ϕ is made up of

sixteen partitions corresponding to four partitions of the state vector

$$\mathbf{x}(t) = [\mathbf{s}(t),\ \lambda(t)]^T = [\mathbf{s}_1(t),\mathbf{s}_2(t),\lambda_1(t),\lambda_2(t)]^T \tag{9.40}$$

The transformation which maps modal space variables into configuration space variables can be shown to be [refs. 10 and 11]

$$\mathbf{y}(t) = \mathcal{O}\mathbf{x}(t) \tag{9.41}$$

where $\mathbf{y}(t) = [\xi(t),\dot{\xi}(t),\Lambda_1(t),\Lambda_2(t)]^T$ is the configuration space state vector, $\mathcal{O}$ is the block diagonal matrix

$$\mathcal{O} = \text{Block Diag. } (E,E,ME,ME) \quad , \quad \mathcal{O}^{-1} = \text{Block Diag. } (E^TM,E^TM,E^T,E^T), \tag{9.42a,b}$$

E is defined by Eq. 9.16, and M is defined by Eq. 9.15. The transformation matrix $\mathcal{O}$ of Eq. 9.42a is derived by equating the optimal control necessary conditions obtained using the configuration space equation of motion given by Eq. 9.15, and the modal space equation of motion given by Eq. 9.20; the details of the derivation can be found in Refs. 10 and 11. The elegant non-numerical inverse $\mathcal{O}^{-1}$ of Eq. 9.42b is a consequence of the orthogonality condition of Eq. 9.19.

In preparing to determine the configuration space state transition matrix, we introduce Eq. 9.41 into Eq. 9.33, to obtain

$$\mathcal{O}^{-1}\mathbf{y}(t) = \phi(t,t_o)\mathcal{O}^{-1}\mathbf{y}(t_o) \tag{9.43}$$

from which it follows that

$$\mathbf{y}(t) = \Phi(t,t_o)\mathbf{y}(t_o) \tag{9.44}$$

where

$$\Phi(t,t_o) = \mathcal{O}\phi(t,t_o)\mathcal{O}^{-1}, \tag{9.45}$$

and $\Phi(t,t_o)$ is the desired configuration space state transition matrix. To obtain the free final angle transversality condition, we recall from Section 6.2 that the general free final time and free final state transversality condition is given by

$$[\frac{\partial H}{\partial \mathbf{s}}|_f - \Lambda_f]^T\delta\mathbf{s}_f + [H_f + \frac{\partial H}{\partial t}|_f]\delta t_f = 0 \tag{9.46}$$

Specializing Eq. 9.46 for the case of a fixed time ($\delta t_f = 0$), free final angle maneuver using the performance index given by Eq. 9.25, then Eq. 9.46 becomes

$$[\frac{\partial H}{\partial \mathbf{s}}|_f - \Lambda_f]^T \delta \mathbf{s}_f = 0 \tag{9.47a}$$

where, since all final conditions other than Θ_f are specified, we have

$$\delta \mathbf{s}_f^T = [\delta\theta_f, \delta\eta_{1f}, \ldots, \delta\eta_{nf}, \delta\dot{\theta}_f, \delta\dot{\eta}_{1f}, \ldots, \delta\dot{\eta}_{nf}] = [\delta\theta_f, 0, 0, \ldots, 0] \tag{9.47b}$$

Recognizing that the Hamiltonian of Eq. 9.26 does not depend explicitely upon $\mathbf{s}_f$, we see that Eq. 9.47a becomes

$$\Lambda_f^T \delta \mathbf{s}_f = 0 \tag{9.48a}$$

which reduces to

$$\Lambda_{1f} \delta\theta_f = 0 \tag{9.48b}$$

where Λ_{1f} is the first element of Λ_f. Since $\delta\theta_f$ is arbitrary in Eq. 9.48b we conclude that the free final angle transversality condition is given by

$$\Lambda_{1f} \triangleq 0 \tag{9.49}$$

Thus, the end conditions $\theta_o, \dot{\theta}_o, \dot{\theta}_f, \eta_o, \dot{\eta}_o, \eta_f, \dot{\eta}_f$, and Λ_{1f} comprise the $4(n + 1)$ boundary conditions necessary for defining the optimal control solution for the free final angle problem.

9.4.5 Solution for the Initial Co-States for the Free Final Angle Maneuver Problem

To obtain the solution for the initial co-states we set $t = t_f$ in Eq. 9.44, yielding:

$$\mathbf{y}(t_f) = \Phi(t_f, t_o)\mathbf{y}(t_o) \tag{9.50}$$

Recalling the known initial and final boundary conditions, we define the terminal boundary condition vectors as follows:

$$\sigma_o = [y_1(t_o) \ \ldots \ y_{2m}(t_o)]^T \ , \quad (2m \times 1) \tag{9.51a}$$

and

$$\sigma_f = [y_2(t_f) \ \ldots \ y_{2m+1}(t_f)]^T \ , \quad (2m \times 1) \tag{9.51b}$$

where $m = n + 1$. From Eqs. 9.50, 9.51a, and 9.51b it follows that the linear

system to be solved for Λ_o can be written as

$$\sigma_f = C\sigma_o + D\Lambda_o \tag{9.52}$$

where the elements of C and D are

$$C_{i-1,j} = \Phi_{ij}(t_f,t_o) \quad , \quad \begin{bmatrix} i = 2, \ldots, 2m+1 \\ j = 1, \ldots, 2m \end{bmatrix}$$

$$D_{i-1,j-2m} = \Phi_{ij}(t_f,t_o) \quad , \quad \begin{bmatrix} i = 2, \ldots, 2m+1 \\ j = 2m+1, \ldots, 4m \end{bmatrix}$$

Rearranging Eq. 9.52, we have

$$D\Lambda_o = \sigma_f - C\sigma_o \tag{9.53}$$

where Eq. 9.53 can be solved for Λ_o using either Gaussian elimination or a similar reduction algorithm for solving linear systems. Equation 9.53 thus provides the basis for the solution for the configuration space initial co-states. Recalling Eq. 9.41, the modal space state and co-state initial conditions are obtained from the following transformation

$$x(t_o) = \Theta^{-1}y(t_o) \tag{9.54}$$

where we have the explicit non-numerical inverse transformation of Eq. 9.42b. Equation 9.54 provides the complete set of initial conditions required for the free final angle attitude maneuver. The time histories for the optimal control problem are obtained most efficiently by using the recursive formulas of Eq. 9.38, subject to the initial state and co-state boundary conditions given by Eq. 9.54. Example maneuvers are provided in Section 9.6.

9.5 NONLINEAR OPTIMAL LARGE-ANGLE MANEUVERS FOR FLEXIBLE SPACECRAFT

9.5.1 Equations of Motion and Optimal Control Formulation

We are now interested in solving the nonlinear version of the linear problem treated in Sections 9.4.1 through 9.4.3, where we seek to retain the rotational stiffening term $\dot{\theta}^2M^*_\eta$ in Eq. 9.14. The equations of motion are

$$I^{*}\ddot{\theta} + \mathbf{M}_{\theta\eta}^{T}\ddot{\eta} = u_1 + 4u_2 \tag{9.55}$$

$$\mathbf{M}_{\theta\eta}\ddot{\theta} + M_{\eta\eta}\ddot{\eta} + [K_{\eta\eta} + \alpha\dot{\theta}^2 M^{*}]\eta = Fu \tag{9.56}$$

where we have arbitrarily introduced the continuation (or homotopy) parameter α, in order to control the participation of the nonlinear term. Following the pattern of Section 8.5.5, we introduce discrete α_i-values ($\alpha_0 = 0 < \alpha_1 < \alpha_2 \cdots \alpha_{n-1} < 1$) to determine neighboring optimal solutions (the true value is $\alpha = 1$). The basic idea is to use: (i) the solution for $\lambda(t_0)$ provided by Eq. 9.37 as the starting solution for the continuation method; and (ii) to solve a sequence of neighboring problems where the final problem is the nonlinear problem of interst (i.e. $\alpha = 1$).

Upon making the same coordinate transformations $[(\theta,\eta) = (\xi) \rightarrow (s)]$ which uncoupled the linear problem (Section 9.3), we obtain

$$\ddot{s}_1 + [\Delta]s_1 = Du - \alpha(\mathbf{W}^T\dot{s}_1)^2 L s_1 \tag{9.57}$$

where

$$\dot{\theta} = \mathbf{W}^T\dot{\mathbf{s}} \; ; \; L = E^T\begin{bmatrix} 0 & 0 \\ 0 & m^{*} \end{bmatrix} E \; ; \; D = E^T\begin{bmatrix} 1 & 4 \\ 0 & F \end{bmatrix}$$

$$\mathbf{W} = E^T[1 \;\; 0^T]^T = [E_{11}E_{12} \cdots E_{1m}]$$

or

$$\dot{\mathbf{s}} = A(\mathbf{s},\alpha)\mathbf{s} + Bu \tag{9.58}$$

where

$$A(\mathbf{s},\alpha) = \begin{bmatrix} 0 & I \\ A_{21}(\mathbf{s},\alpha) & 0 \end{bmatrix} \; ; \; B = \begin{bmatrix} 0 \\ D \end{bmatrix} \; ; \; \mathbf{s} = \begin{Bmatrix} s_1 \\ s_2 \end{Bmatrix} \; ; \; \mathbf{u} = \begin{Bmatrix} u_1 \\ u_2 \end{Bmatrix}$$

$$A_{21}(\mathbf{s},\alpha) = -\Delta - \alpha(\mathbf{W}^T s_2)^2 L$$

$$\Delta = \text{Diag.}(\lambda_1^2 \; \ldots \; \lambda_N^2)$$

Defining the optimal control performance index exactly as in the linear problem (i.e., Section 9.3) leads to the state and co-state differential equations which are summarized as:

State Equations

$$\dot{\mathbf{s}} = A(\mathbf{s},\alpha)\mathbf{s} - BW_{uu}^{-1}B^T\lambda \tag{9.59}$$

Co-state Equations

$$\dot{\lambda} = -W_{ss}\mathbf{s} - C(\mathbf{s},\alpha)\lambda \tag{9.60}$$

where

$$C(\mathbf{s},\alpha) = \begin{bmatrix} 0 & A_{21}^T(\mathbf{s},\alpha) \\ I & -2\alpha(\mathbf{W}^T\mathbf{s}_2)^2 D\mathbf{s}_1^T L \end{bmatrix}$$

with the optimal control given by

$$\mathbf{u} = -W_{uu}^{-1}B^T\lambda \tag{9.61}$$

9.5.2 Continuation Method for the Solution of the Nonlinear TPBVP

For Eqs. 9.59 and 9.60, we typically have a priori knowledge of the initial state $\mathbf{s}(t_o) = \mathbf{s}_o$ and the desired final state $\mathbf{s}(t_f) = \mathbf{s}_f$, but we lack boundary conditions on $\lambda(t)$; thus we arrive at a nonlinear two-point boundary-value problem.

The parameter α was introduced (or embedded) in Eqs. 9.59 and 9.60 in order to define a one parameter family of problems, where we know how to noniteratively compute the solution for $\alpha = 0$. However, we are in fact only interested in the solution for $\alpha = 1$.

In a more general context, the motivation for introducing the parameter α in Eqs. 9.59 and 9.60 comes about from the following simple observation. If it is very difficult to directly obtain a solution for a vector $\mathbf{x}$ satisfying the nonlinear vector equation

$$F(\mathbf{x}) = 0, \tag{9.62}$$

the numerical solution of Eq. 9.62 can frequently be obtained, as shown in other examples of Chapter 8, by solving the family of problems

$$G(\mathbf{x},\alpha) = 0 \tag{9.63}$$

where α is a parameter which varies from 0 to 1, and $F(\mathbf{x}) = 0$ has been embedded in $G(\mathbf{x},\alpha) = 0$.

The family $\mathbf{G}(\mathbf{x},\alpha)$ is constructed such that (i) $\mathbf{G}(\mathbf{x},1) = \mathbf{F}(\mathbf{x})$, (ii) $\mathbf{x}_0$ is an easily calculated (usually) and ideally (unique) fixed point solution of $\mathbf{G}(\mathbf{x},0) = \mathbf{0}$, and (iii) $\mathbf{G}(\mathbf{x},\alpha)$ is a continuous function of α.

Upon introducing the sequence of neighboring α-values $\{\alpha_0 = 0 < \alpha_1 < \alpha_2 < \ldots < \alpha_{n-1} < \alpha_n = 1\}$, we define the following sequence of neighboring nonlinear TPBVP's:

$$\mathbf{G}(\mathbf{x}_i,\alpha_i) = \mathbf{0} \quad , \quad i = 0,1,2,\ldots,n \tag{9.64}$$

where $\mathbf{x}_i$ denotes the converged solution $\mathbf{x}(\alpha_i)$ for the ith α-value.

To define an algorithm for determining solutions of the sequence of nonlinear TPBVP's defined by Eq. 9.64, we must prescribe: (i) how α_{i+1} is determined given the preceding α_i, and (ii) how starting iteratives are determined for each successive $\mathbf{x}_{i+1}$ given the preceding converged $\mathbf{x}_i$. For $\Delta\alpha_{i+1} = \alpha_{i+1} - \alpha_i$ sufficiently small, excellent starting iteratives for $\mathbf{x}_{i+1}$ at $\alpha = \alpha_{i+1}$ can almost invariably be linearly extrapolated from the previous converged solutions $\mathbf{x}_i$, $\mathbf{x}_{i-1}$ at $\alpha = \alpha_i, \alpha_{i-1}\ldots$, respectively (exceptions may occur if, for example, a bifurcation point or a turning point is encountered). Accordingly, the following linear extrapolation equation is used for the example problems in Section 9.6:

$$\hat{\mathbf{x}}_{i+1} \tilde{=} \mathbf{x}_i + (\Delta\mathbf{x}_i/\Delta\alpha_i)\Delta\alpha_{i+1} \tag{9.65}$$

where $\hat{\mathbf{x}}_{i+1}$ denotes the extrapolated estimate of $\mathbf{x}_{i+1}$, $\Delta\mathbf{x}_i/\Delta\alpha_i$ denotes the backward finite difference approximation for the derivative with respect to α of the converged solution for $\mathbf{x}_i$, which is obtained by substituting the converged $\mathbf{x}_i$, $\mathbf{x}_{i-1}$ into

$$\Delta\mathbf{x}_i/\Delta\alpha_i = (\mathbf{x}_i - \mathbf{x}_{i-1})/(\alpha_i - \alpha_{i-1}), \tag{9.66}$$

and $\Delta\alpha_{i+1} = \alpha_{i+1} - \alpha_i$.

Since $\mathbf{G}(\mathbf{x}_i,\alpha_i)$ is in general nonlinear, the extrapolated estimate of $\mathbf{x}_{i+1}$ given by Eq. 9.65 must generally be iteratively refined using a successive approximation strategy. Of course, a number of iterative algorithms are

available for solving nonlinear systems of equations; however, for the nonlinear example maneuvers of this section, the class of algorithms known as Quasi-Newton methods have been successfully applied (see refs. 12, 13, 14 for a detailed discussion of Quasi-Newton methods).

Clearly, in Eq. 9.64, the number of intermediate α-values that are introduced can be either pre-set or adaptively determined during the iterative procedure. Examples of different types of α-adjustment procedures used in continuation methods can be found in Schmidt (ref. 15), Deuflhard, et al. (ref. 16), Junkins and Turner (ref. 17), Turner (ref. 10), and Roberts, Shipman, Roth (ref. 18), and Turner and Chun (ref. 23). However, for the example maneuvers discussed in Section 9.6, a pre-set selection of α-values has proven successful. Nevertheless, if difficult problems are encountered, then a simple and usually effective procedure is to simply halve $\Delta\alpha_k$, and thereby make α_{k+1} closer to the previous α_k for which a converged solution has been obtained.

As with any nonlinear iteration problem, we must always be alert to the possibility that bifurcation points or other singularities may be encountered during the solution process, which may defeat the algorithm as formulated above. The Chow-Yorke homotopy algorithm [19], (as implemented by Watson [20,21] and further demonstrated by Dunyak, Junkins, and Watson [22]) is an expensive but very useful method if the particular application fails to converge due to the presence of turning points. In essence, this method involves two convergence enhancing devices: (1) In lieu of (α), arc length (s), along the n + 1 dimensioned trajectory ($\mathbf{x}(s)$, $\alpha(s)$) is used as the independent variable of the continuation. (2) Differential equations are derived and solved for $\mathbf{x}(s)$, $\alpha(s)$ with high precision maintained at all s-values until s_f is found such that $\alpha(s_f) = 1$. Of course, no algorithm can be expected to extract a solution if none exists.

In the developments above, we have assumed the ideal situation; namely, that $\mathbf{G}(\mathbf{x},\alpha)$ is a continuous single-valued function of both $\mathbf{x}$ and α.

For the nonlinear problem of interest, we identify the nonlinear operators $\mathbf{F}(\mathbf{s},\lambda) = \mathbf{G}(\mathbf{s},\lambda,\alpha)$ as

$$\mathbf{G}(\mathbf{s},\lambda,\alpha) = \begin{Bmatrix} \dot{\mathbf{s}} - \mathbf{A}(\mathbf{s},\alpha) + \mathbf{B}\mathbf{W}_{uu}^{-1}\mathbf{B}^T\lambda \\ \dot{\lambda} + \mathbf{W}_{ss}\mathbf{s} + \mathbf{C}(\mathbf{s},\alpha)\lambda \\ \mathbf{s}_f - \mathbf{s}(\mathbf{s}_o,\lambda_o,\alpha,t_f) \end{Bmatrix} = \begin{Bmatrix} 0 \\ 0 \\ 0 \end{Bmatrix} \tag{9.67}$$

We note in Eq. 9.67 that $\mathbf{s}_o = \mathbf{s}(t_o)$ is known for all α-values, $\lambda_o = \lambda(t_o)$ is known a priori only for $\alpha = 0$, and extrapolated estimates are available for $\lambda_o(\alpha)$ from Eq. 9.65 for all α-values greater than zero. Thus, for $\alpha \neq 0$, the unknown vector (to be determined by iteration) in Eq. 9.67 is λ_o. Accordingly, we introduce a "successive approximation" strategy in order to iteratively solve the state and co-state differential equations for the λ_o which satisfies $\mathbf{s}_f - \mathbf{s}(\mathbf{s}_o,\lambda_o,\alpha_k,t_f) = \mathbf{0}$ for $k > 0$.

The "successive approximation" strategy used for solving the nonlinear TPBVP, for the homotopy chain parameters $\alpha_k(k=1,\ldots,n)$, is developed as follows.

Let the approximate initial co-state be denoted by

$$\hat{\lambda}_o \overset{\Delta}{=} \lambda(t_o) \tag{9.68}$$

The differential correction strategy seeks the correction vectors, $\Delta\lambda$, which satisfies the terminal constraint

$$\mathbf{s}_f - \mathbf{s}(\mathbf{s}_o,\hat{\lambda}_o + \Delta\lambda,\alpha_k,t_f) = \mathbf{0} \tag{9.69}$$

However, since the state and co-state differential equations are nonlinear, a single step solution for $\Delta\lambda$ from Eq. 9.69 is not in general possible. As a result, we expand Eq. 9.69 in a first-order Taylor series about $(\mathbf{s}_o,\hat{\lambda}_o,\alpha_k,t)$, leading to

$$\Delta\mathbf{s}_f = \phi_{s\lambda}\Delta\lambda \tag{9.70}$$

where

$$\Delta s_f = s_f - s(s_o, \hat{\lambda}_o, \alpha_k, t_f) \tag{9.71}$$

is the residual vector and

$$[\phi_{s\lambda}]_{ij} = \partial s_i(t_f)/\partial \lambda_j(t_o) \quad , \begin{cases} i = 1, \ldots, 2m \\ j = 1, \ldots, 2m \end{cases} \tag{9.72}$$

is the ijth element of the Jacobian where $s(s_o, \hat{\lambda}_o, \alpha_k, t_f)$ and $\phi_{s\lambda}$ result from integrating Eqs. 9.59 and 9.60, and the associated nonlinear state transition matrix. The matrix differential equation for computing the nonlinear state transition matrix is presented in Section 9.5.3. The initial co-state correction, $\Delta\lambda$, is obtained from Eq. 9.70 using any convenient linear equation solver (e.g., Gaussian elimination).

The Newton algorithm (shooting method) for refining approximate initial co-states for each α-value, consists of the recursive solution of Eq. 9.70 for $\Delta\lambda$ until the weighted norm of Δs is less than some small prescribed value (typically, only one to three corrections are required). Once the iterative solution for $\hat{\lambda}_o$ has converged for the kth α-value, α_k is incremented as follows:

$$\alpha_{k+1} \overset{\Delta}{=} \alpha_k + \Delta\alpha_k \qquad (k \geq 0) \tag{9.73}$$

The starting co-state estimate, $\hat{\lambda}_{0,k+1}$, is obtained from the first-order extrapolation defined by Eq. 9.65, where $\lambda_{0,k}$ replaces x_k. The combined continuation and differential correction process is outlined in Figure 9.3.

The following pre-set sequence of α-values has been used in the computed example maneuvers of Section 9.6

$$\{\alpha_o, \alpha_1, \alpha_2, \alpha_3, \alpha_4, \alpha_5\} = \{0.0, 10^{-3}, 10^{-2}, 0.5, 0.75, 1.0\} \tag{9.74a}$$

or

$$\{\Delta\alpha_o, \Delta\alpha_1, \Delta\alpha_2, \Delta\alpha_3, \Delta\alpha_4\} = \{10^{-3}, 9\times10^{-3}, 0.49, 0.25, 0.25\} \tag{9.74b}$$

For more nonlinear problems, of course, smaller α-increments must be taken.

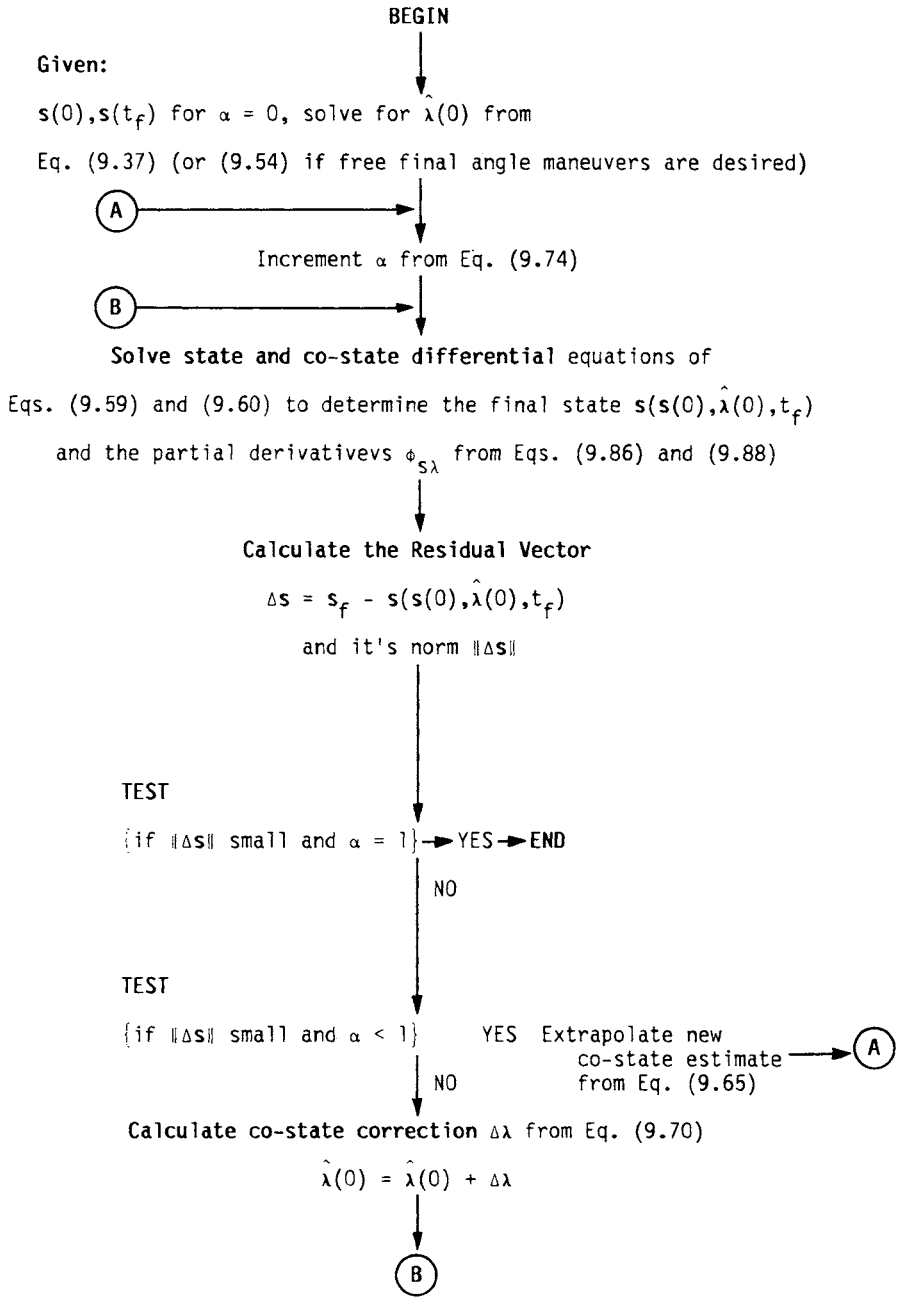

Figure 9.3 Differential Correction and Continuation Process for Determination of Optimal Nonlinear Maneuvers

Local singularities appear possible in the solution for $\Delta\lambda$ from Eq. 9.70, due to rank deficiencies in $\phi_{s\lambda}$; however, for the single-axis maneuvers considered to date no such difficulties have been encountered.

A more common practical difficulty in this class of problems is that the calculation of the nonlinear state transition matrix is expensive; however, numerical integration is usually stable. For the (occasionally encountered) case of very stiff differential equations, standard numerical methods may fail if the integration time $(t_f - t_o)$ exceeds a critical value; leading to overflows and/or a loss of linear independence in the computed solutions. One simple ad hoc test (we've used successfully) consists checking for satisfaction of the following inequality

$$\nu(t_f - t_o) \leq \varepsilon$$

where ν is the real part of the largest positive eigenvalue of the Ω matrix in Eq. 9.32 and ε is small tolerance parameter. The selection of ε above insures that matrix norm of the state transition matrix of Eq. 9.33 satisfies the inequality

$$\|\phi(t,t_o)\| < \exp(\varepsilon)$$

thus bounding the growth in the elements of $\phi(t,t_o)$. Should the above or other "stiffness tests" not be satisfied, we suggest two remedial steps:

(1) decrease the maneuver time interval $(t_f - t_o)$; and/or

(2) adjust the state and control weighting matrices W_{ss} and W_{uu}, in order to decrease the bandwidth of the eigenvalue spectrum of Ω in Eq. 9.32. One can be guided in this weight process by calculating the eigenvalue sensitivities using the explicit eigenvalue partial derivatives

$$\frac{\partial \lambda_i}{\partial W_\ell} = \ell_i^T \frac{\partial \Omega}{\partial W_\ell} r_i \qquad i = 1,2,\ldots,n,\ \ell = 1, \ldots, \gamma$$

where the eigenvalues (λ_i) and eigenvectors (r_i, ℓ_i) of Ω satisfy

$$\lambda_i r_i = \Omega r_i \quad , \quad \lambda_i \ell_i = \Omega^T \ell_i \quad , \quad i = 1,2,\ldots,n$$

with

$$\Omega = \begin{bmatrix} A & -BW_{uu}^{-1}B^T \\ -W_{ss} & -A^T \end{bmatrix}$$

$$\frac{\partial \Omega}{\partial W_\ell} = \begin{bmatrix} 0 & BW_{uu}^{-1}\dfrac{\partial W_{uu}}{\partial W_\ell}W_{uu}^{-1}B^T \\ -\dfrac{\partial W_{ss}}{\partial W_\ell} & 0 \end{bmatrix}$$

and

W_ℓ is any element of either W_{ss} or W_{uu}.

9.5.3 State Transition Matrix of the Nonlinear System

In order to produce the required partial derivatives in Eq. 9.72, we must numerically integrate the nonlinear system's state transition matrix. The differential equation for the state transition matrix is obtained as follows.

First, we consider the vector $z^*(t)$ defined by

$$z^*(t) = [s(t), \lambda(t)]^T \tag{9.75}$$

where the time derivative of $z^*(t)$ is known to be

$$\dot{z}^*(t) = F(z^*(t),t) \tag{9.76}$$

and F is given by Eqs. 9.59 and 9.60 as

$$F(z^*(t),t) = \begin{bmatrix} A(s(t),\alpha) & -BW_{uu}^{-1}B^T \\ -W_{ss} & C(s(t),\alpha) \end{bmatrix} \begin{Bmatrix} s(t) \\ \lambda(t) \end{Bmatrix} \tag{9.77}$$

where α is the artificially introduced continuation parameter.

From Eq. 9.76, we are lead to the formal solution for $z^*(t)$:

$$z^*(t) = z^*(t_o) + \int_{t_o}^{t} F(z^*(\tau),\tau)d\tau \tag{9.78}$$

Upon taking the partial derivative of Eq. 9.78 with respect to $z^*(t_o)$, we obtain

$$\frac{\partial z^*(t)}{\partial z^*(t_o)} = \frac{\partial z^*(t_o)}{\partial z^*(t_o)} + \int_{t_o}^{t} \frac{\partial F(z^*(\tau),\tau)}{\partial z^*(\tau)} \frac{\partial z^*(\tau)}{\partial z^*(t_o)} d\tau \quad , \tag{9.79}$$

where the initial condition for

$\partial z_i^*(t)/\partial z_j^*(t_o)$ is given by

$$\frac{\partial z_i^*(t_o)}{\partial z_j^*(t_o)} = \delta_{ij} \quad , \quad i = 1, \ldots, 4m, \; j = 1, \ldots, 4m \tag{9.80}$$

and δ_{ij} is the kronecker delta symbol.

Defining the (i,j)th element of the state transition matrix as

$$\phi_{ij}(t,t_o) = \frac{\partial z_i^*(t)}{\partial z_j^*(t_o)}$$

it follows that the time derivative of Eq. (9.79) can be written as

$$\dot{\phi}(t,t_o) = F(z^*(t),t)\phi(t,t_o) \; , \; \phi(t_o,t_o) = I \tag{9.81}$$

where

$$F_{ij} = \frac{\partial F_i(z^*(t),t)}{\partial z_j^*(t)} \quad , \quad i = 1, \ldots, 4m, \; j = 1, \ldots, 4m$$

Moreover, by defining the matrix partitions of ϕ and F as

$$\phi = \begin{bmatrix} \phi_{ss} & \phi_{s\lambda} \\ \phi_{\lambda s} & \phi_{\lambda\lambda} \end{bmatrix} \tag{9.82}$$

and

$$F = \begin{bmatrix} F_{ss} & F_{s\lambda} \\ F_{\lambda s} & F_{\lambda\lambda} \end{bmatrix} \tag{9.83}$$

we obtain the following matrix differential equations for the partitions of ϕ:

$$\dot{\phi}_{ss} = F_{ss}\phi_{ss} + F_{s\lambda}\phi_{\lambda s} = G_1(\phi_{ss},\phi_{\lambda s}) \tag{9.84}$$

$$\dot{\phi}_{s\lambda} = F_{ss}\phi_{s\lambda} + F_{s\lambda}\phi_{\lambda\lambda} = G_2(\phi_{s\lambda},\phi_{\lambda\lambda}) \tag{9.85}$$

$$\dot{\phi}_{\lambda s} = F_{\lambda s}\phi_{ss} + F_{\lambda\lambda}\phi_{\lambda s} = G_3(\phi_{ss},\phi_{\lambda s}) \tag{9.86}$$

$$\dot{\phi}_{\lambda\lambda} = F_{\lambda s}\phi_{s\lambda} + F_{\lambda\lambda}\phi_{\lambda\lambda} = G_4(\phi_{s\lambda},\phi_{\lambda\lambda}) \tag{9.87}$$

From Eq. 9.70, we observe that only the $\phi_{s\lambda}$ partition of ϕ is required for

computing the co-state correction vector $\Delta\lambda$. However, from Eq. 9.85 it follows that $\dot{\phi}_{s\lambda}$ is only a function of $\phi_{s\lambda}$ and $\phi_{\lambda\lambda}$. Furthermore, on checking Eq. 9.87 we find that $\dot{\phi}_{\lambda\lambda}$ is only a function of $\phi_{s\lambda}$ and $\phi_{\lambda\lambda}$. As a result, since Eqs. 9.85 and 9.87 are simply functions of $\phi_{s\lambda}$ and $\phi_{\lambda\lambda}$, only Eqs. 9.85 and 9.87 are required to produce $\phi_{s\lambda}$; thus reducing by half the number of matrix partition calculations required. Nonetheless, further significant savings can be realized if the special sparse structure of the matrix partitions of Eq. 9.83 is taken into account, while performing the arithmetic implicit in Eqs. 9.85 and 9.87.

Using the techniques described above, as the number of modes retained in the dynamical model becomes large, the savings in the required computational effort to produce $\phi_{s\lambda}$ has been found to approach 75%.

9.6 EXAMPLE MANEUVERS

We now consider example maneuvers for the configuration shown in Figure 9.1, using the above formulations (see ref. 23). For all cases, we have assumed the following configuration parameters: The inertia of the undeformed structure, $\hat{I}$, is 7000 kg-m^2; the mass/length of the four identical elastic appendages, ρ, is 0.0004 kg/m; the length of each cantilevered appendage, L, is 150 m; the flexural rigidity of the cantilevered appendages, EI, is 1500 kg-m^3/s^2 for cases (2-4) (Table 9.1); and the radius of the rigid hub, r, is 1m. In the integrations over the mass and stiffness distributions, the radius of the hub is not neglected in comparison to the appendage length. We have adopted as assumed modes the comparison functions

$$\phi_p(x - r) = 1 - \cos\frac{p\pi(x - r)}{L} + \frac{1}{2}(-1)^{p+1}\left(\frac{p\pi(x - r)}{L}\right)^2 \qquad (9.88)$$

$$(p = 1,2,\ldots,\infty)$$

which satisfy the geometric and physical boundary conditions

$$\phi_p|_{x=r} = \phi_p'|_{x=r} = \phi_p''|_{x=r+L} = \phi_p'''|_{x=r+L} = 0 \qquad (9.89)$$

of a clamped-free appendage.

Table 9.1 Description of Test Case Maneuvers

Case No	Qualitative Description	No. of Modes N	θ_o rad	$\dot{\theta}_o$ rad/sec	θ_f rad	$\dot{\theta}_f$ rad/sec	No. of Controls	W_{uu}	W_{ss}
1	Rigid Appendages Rest-to-Rest Maneuver t_f = 60 sec	0	0	0	π	0	1	1	[0]
2	Linear Kinematics Rest-to-Rest Maneuver t_f = 60 sec	2	0	0	π	0	1	1	$[\hat{I}]^*$
3	Linear Kinematics Rest-to-Rest Maneuver t_f = 60 sec	2	0	0	π	0	1	1	$[\hat{I}]^\dagger$
4	Linear Kinematics Rest-to-Rest Maneuver t_f = 60 sec	2	0	0	π	0	5	[I]	$10^{-2}[\hat{I}]$
5	Linear/Nonlinear Kinematics** Rest-to-Rest Maneuver t_f = 60 sec	4	0	0	π	0	5	[I]	$10^{-5}[\hat{I}]$
6	Linear Kinematics Spinup Maneuver t_f = 60 sec	3	0	0	2π	0.5	5	[I]	$10^{-5}[\hat{I}]$
7	Linear Kinematics Free Final Angle Spinup Maneuver t_f = 60 sec	3	0	0	(free)	0.5	5	[I]	10^{-5}[I]
8	Nonlinear Kinematics Spinup Maneuver t_f = 60 sec	3	0	0	2π	0.5	5	[I]	$10^{-5}[\hat{I}]$
9	Linear Kinematics Spin Reversal Maneuver t_f = 60 sec	3	0	-0.5	2π	0.5	5	[I]	$10^{-4}[\hat{I}]$
10	Linear Kinematics Free Final Angle Spin Reversal Maneuver t_f = 60 sec	3	0	-0.5	(free)	0.5	5	[I]	$10^{-4}[\hat{I}]$
11	Nonlinear Kinematics Spin Reversal Maneuver t_f = 60 sec	3	0	-0.5	2π	0.5	5	[I]	$10^{-4}[\hat{I}]$
12	Linear Kinematics Rest-to-Rest Maneuver t_f = 60 sec	10	0	0	$\pi/18$	0	5	[I]	$10^{-6}[\hat{I}]$

*W_{ss} set to a diagonal matrix

†W_{ss} set to an identity matrix with the first element set to 10^{-2}. This sets a lower weight on the maneuver angle. Then the diagonal matrices are mapped via the equation $W_{ss} + E^T W_{ii} E$ for i = 1,2 for cases 3 through 12.

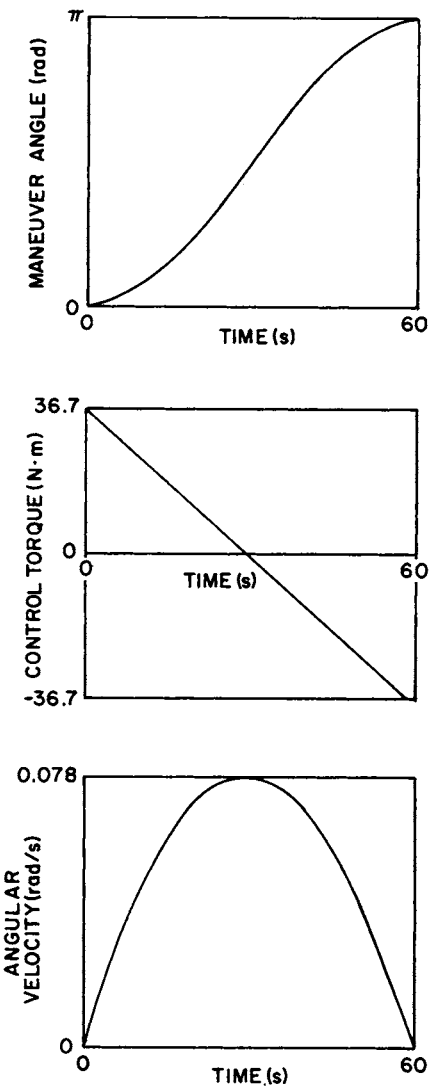

Figure 9.3 Case 1: Rigid Appendages, Rest-to-Rest Maneuver

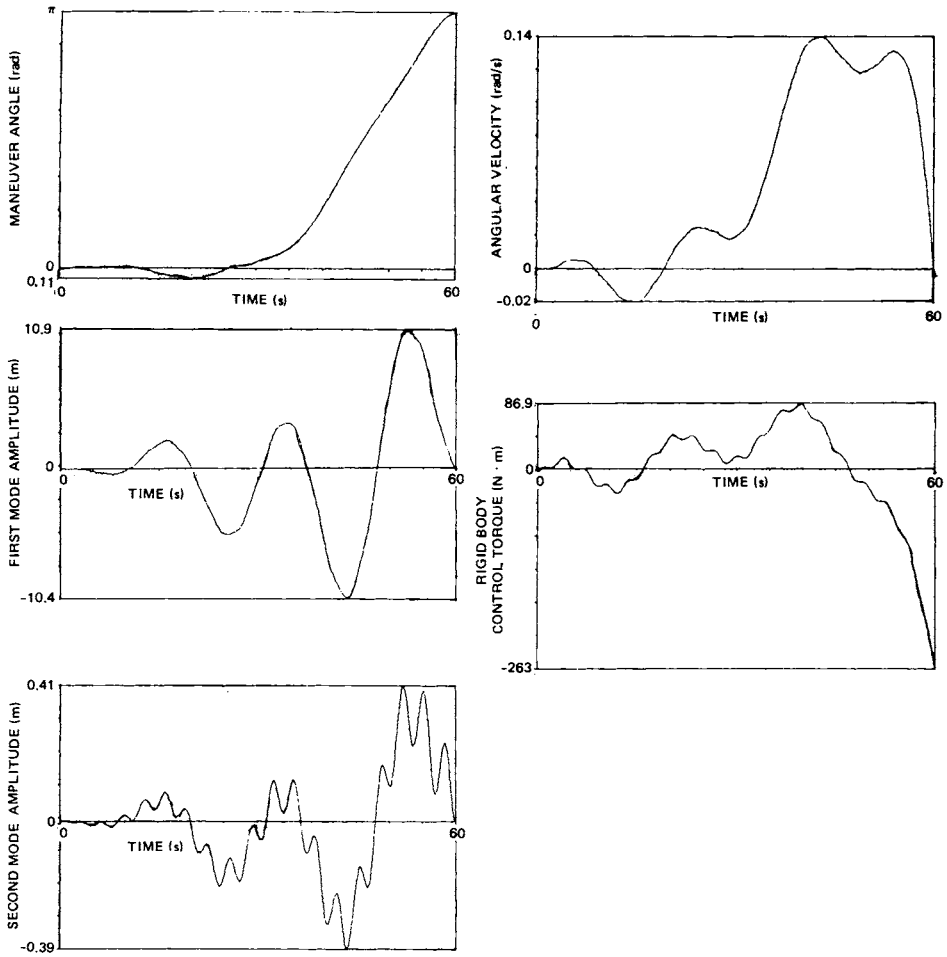

Figure 9.4 Case 2, Rest-to-Rest Maneuver, 2 Modes, 1 Control

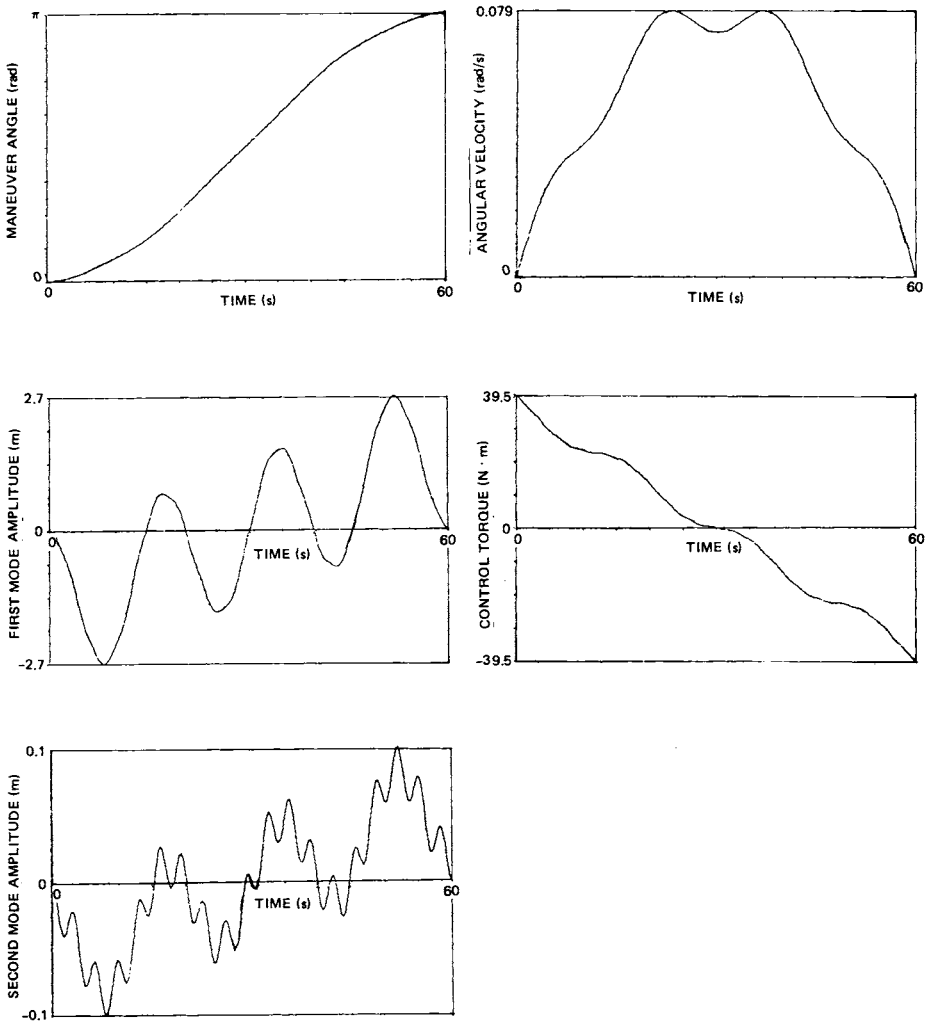

Figure 9.5 Case 3, Rest-to-Rest Maneuver, 2 Modes, 1 Control

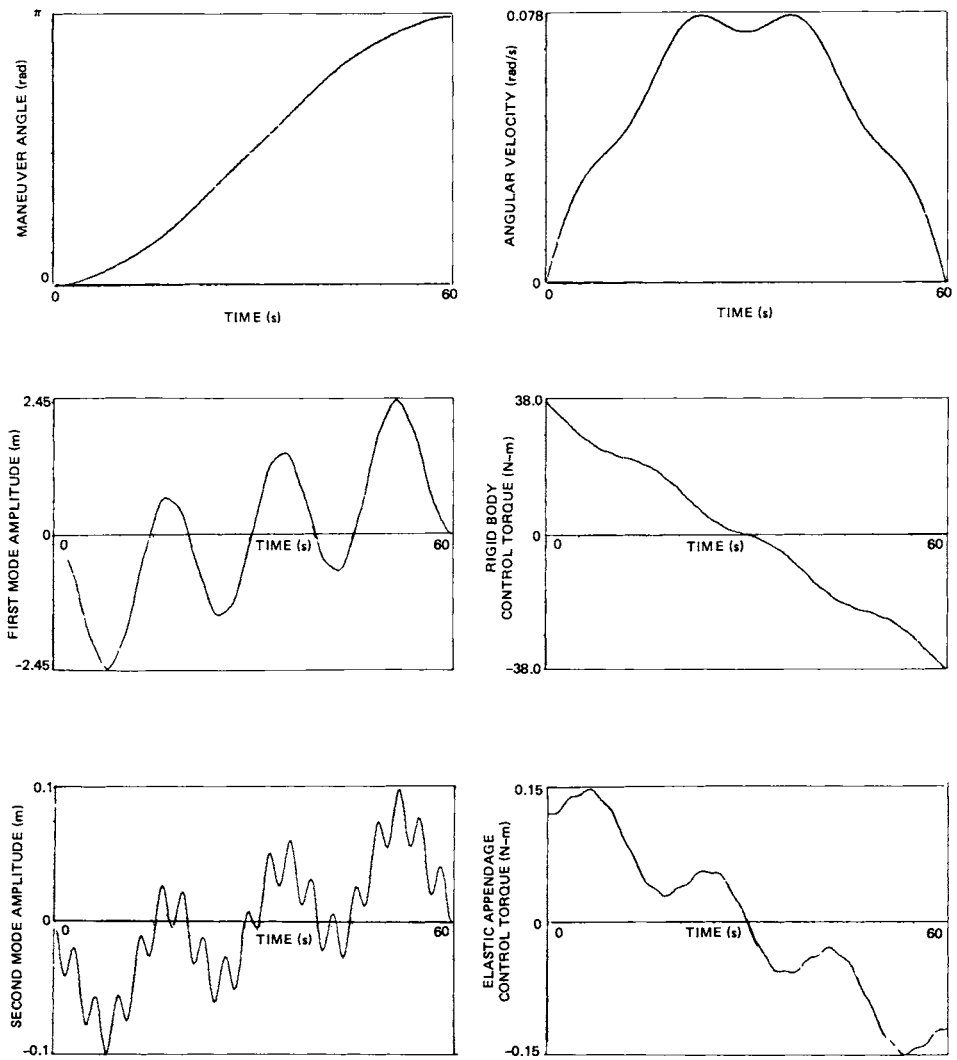

Figure 9.6 Case 4, Rest-to-Rest Maneuver, 2 Modes, 5 Controls

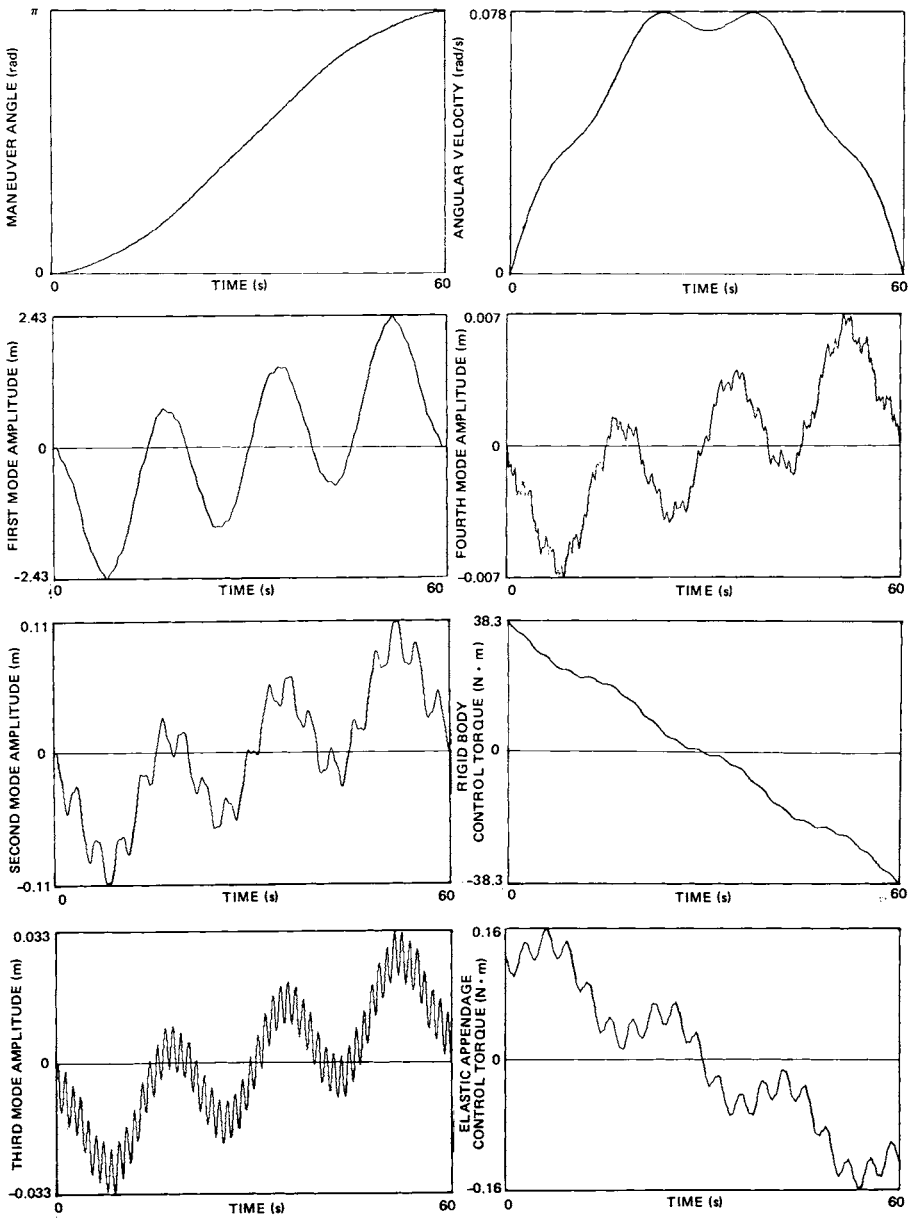

Figure 9.7 Case 5, Linear/Nonlinear, Rest-to-Rest Maneuver, 4 Modes, 5 Controls

With reference to Table 9.1 and Figures 9.3 through 9.14, we consider qualitatively the graphical summaries of the state and control time histories.

Case 1 corresponds to the rigid body case, which is presented for comparison with the flexible body examples.

Case 2 demonstrates that when flexibility effects are taken into account, the resulting control torque profiles are indeed significantly altered.

The boundary conditions for Cases 2 and 3 are identical; the difference between the two maneuvers is the choice of weight matrices W_{ss}. In Case 2 we used a simple diagonal matrix, whereas, for Case 3, we mapped this weight matrix (i.e., $W_{ss} \rightarrow E^T W_{ii} E$ for i = 1,2). We observe that the torque histories for the two cases are very different. In this case it can be seen that the peak torque and modal amplitudes of Case 2 are much larger than those of Case 3; in fact, the peak torque decreases by 570% and the peak structural deflection decreases by 300%! Based on these results, it is clear that careful consideration must be given to weighting matrices selected in the performance index. This observation is consistent with similar results for feedback controls as discussed in Chapter 6. General techniques for selecting the elements of the weighting matrices is a topic of current interest, and a new approach has been formulated by Bodden, Junkins, and Turner (see ref. 24).

Comparing Case 3 with Case 4, we find that the rigid body torque profile is smoothed out by the addition of one controller on each appendage. The maximum torque required for the appendage control is much less than that required for the hub control. However, in the performance index, the appendage control weight matrix was adjusted in order to assure that the appendage controllers acted as vibration suppressors, and that the rigid hub controller acted to supply the primary reorientation torque. We also find that the hub angular velocity and appendage vibration amplitudes are reduced slightly, for maneuvers where a distributed set of discrete controllers is compared to a

single (hub torque) control case. Furthermore, when nine controls are applied to the vehicle (two on each appendage, one on the hub), we find that the additional appendage controllers have a negligible effect on the torque time histories and the system response (these results are not shown).

As shown in Ref. 11, when the weighting matrix W_{uu} is set to be two orders of magnitude smaller, the peak modal amplitudes are descreased by 200%, even though the peak torque remains relatively unchanged. Unfortunately, the improved performance is often obtained at the expense of increased control system sensitivity to parameter uncertainty. As a result, for real applications, parametric ("robustness") studies should be performed in order to assure satisfactory system performance in the presence of the anticipated range of model uncertainty.

Referring to Case 5, we find that the modal amplitudes, torque histories, and the vehicle angular velocities are identical (to plotting accuracy) for the linear and nonlinear cases. However, when we compare the results of Cases 4 and 5, we observe that the higher modes have little effect on the overall system response. This result indicates, for this example, that the low order model can be used to adequately represent the vehicle for the purpose of determining controls for slewing maneuvers. Of course, a general conclusion on truncation/spillover cannot be inferred from numerical experiments with a single configuration!

Case 6 is an interesting spin-up maneuver. In particular, notice that a torque reversal is required to match the final boundary conditions. The rigid hub torque profile is smooth due to the presence of the appendage controls. It should be pointed out, however, that the torque reversal phenomenon is a by-product of solving either a fixed time or fixed angle maneuver (see Chapter 6 for similar rigid body results), with a poor or "un-natural" choice for the fixed end conditions.

Case 7 treats the same maneuver as shown in Case 6, except that the free final angle is determined as part of the optimal solution (see Section 9.4.4 for the necessary conditions governing this maneuver). We observe the three following qualitative improvements in the resulting maneuver:

(1) the peak modal amplitudes decrease by 120%;

(2) the peak torques decrease by 130%; and

(3) the spin reversal phenomena disappears.

On the basis of this and other examples we conclude that if the optimal solution determines the *natural boundary condition* for rigid body angle (i.e., for maneuvers where only the final angular rate is important), the vehicle's controlled performance is usually significantly improved. Of course other performance index choices can also eliminate these problems (e.g., minimum time maneuvers).

Case 8 is the nonlinear version of the Case 6 maneuver. We reach two conclusions on comparing the results of Cases 6 and 8. First, the rotational stiffening effect of the kinematic nonlinearity has decreased the participation of the first mode at the expense of slightly exciting the higher modes. Second, the required rigid body torque has remained unchanged, while the appendage control torques have decreased. Indeed, since the observed differences between the linear and nonlinear solutions are small, it can be anticipated that if slow maneuvers are carried out (i.e., $\dot{\theta}^2$ remains small during the entire maneuver), a linear analysis is adequate for single-axis maneuvers. However, if large structural deflections are of interest, then nonlinear terms must be retained irregardless of the value of $\dot{\theta}^2$.

Case 9 is a spin reversal maneuver which requires the vehicle's angular velocity vector to reverse its algebraic sign. On comparing the results with Case 6, we find that the spin reversal maneuver induces greater flexural deformations in the structure. Furthermore, we observe that the time histories

for the state and control are not symmetric with respect to the midpoint of the maneuver time.

Case 10 is the free final angle maneuver which corresponds to Case 9. As in Case 7, we find significant improvements in the maneuver, especially in terms of reduced peak flexural deflections and peak torque requirements. In addition, we observe that the time histories for the state and control are now symmetric with respect to the midpoint of the maneuver time, which should be contrasted wtih the results of Case 9.

Case 11 is the nonlinear version of Case 9. As in Case 8, the first mode amplitude decreased while the higher modes are excited somewhat more. The peak appendage control torque decreases and the time histories for the various variables are somewhat smoother than in Case 9. This maneuver provides further support for the contention that nonlinear rotational stiffening effects are not significant unless either extremely large deflections or rotation rates are achieved. However the ability (of this approach) to handle this nonlinearity is a basis for optimism when other nonlinear effects are modeled (e.g., nonlinear stress-strain relationships).

Case 12 represents a simple linear rest-to-rest maneuver where ten elastic modes of the structure are controlled. As in Case 5, we have further confirmation of the observation that only the first few elastic modes participate in the system response during the slewing maneuvers considered.

From the results of this section, we can draw the following conclusions:

(1) Flexible body effects significantly influence spacecraft slewing maneuvers;

(2) Selection of the state and control weighting matrices W_{ss} and W_{uu} significantly effects the optimal control torque profiles and the resulting maneuvers;

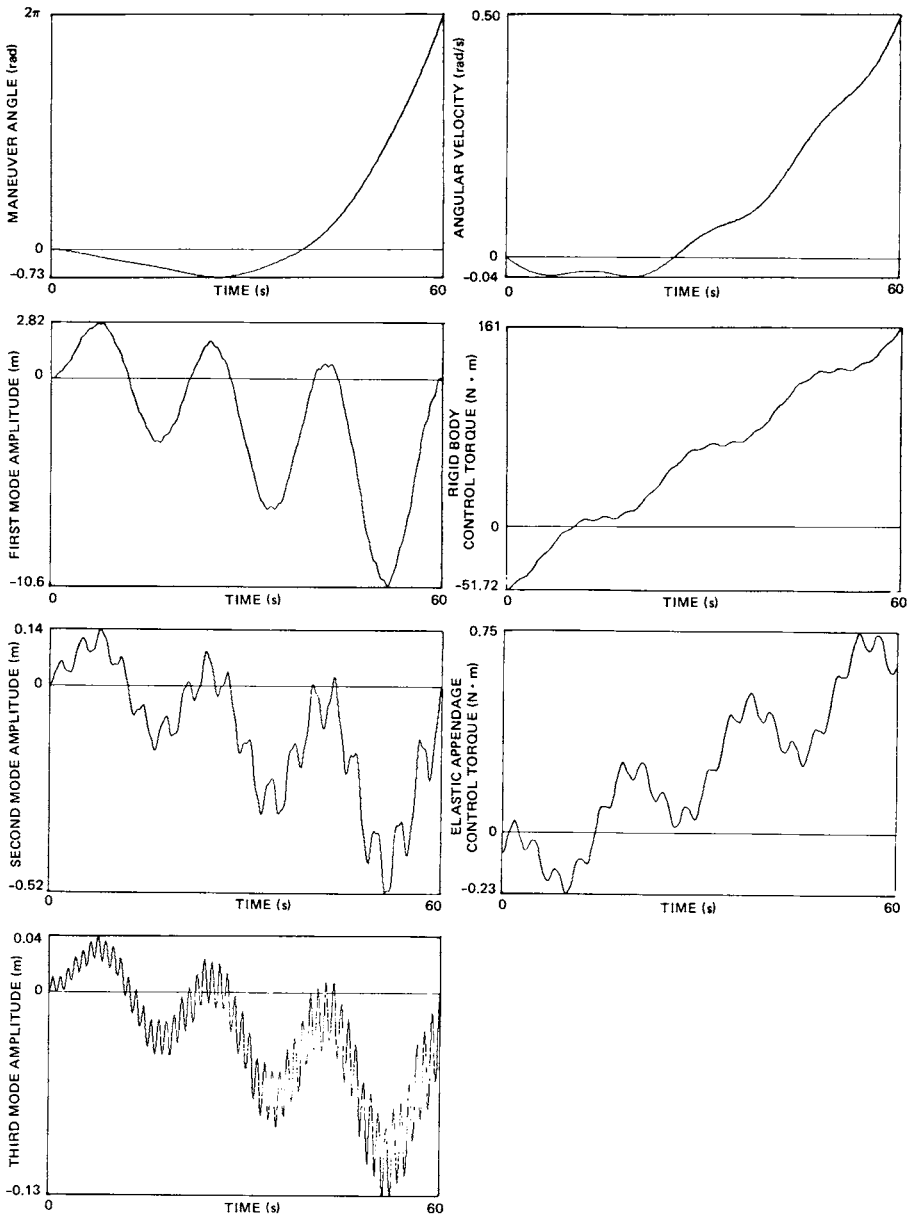

Figure 9.8 Case 6, Linear Spinup Maneuver, 3 Modes, 5 Controls

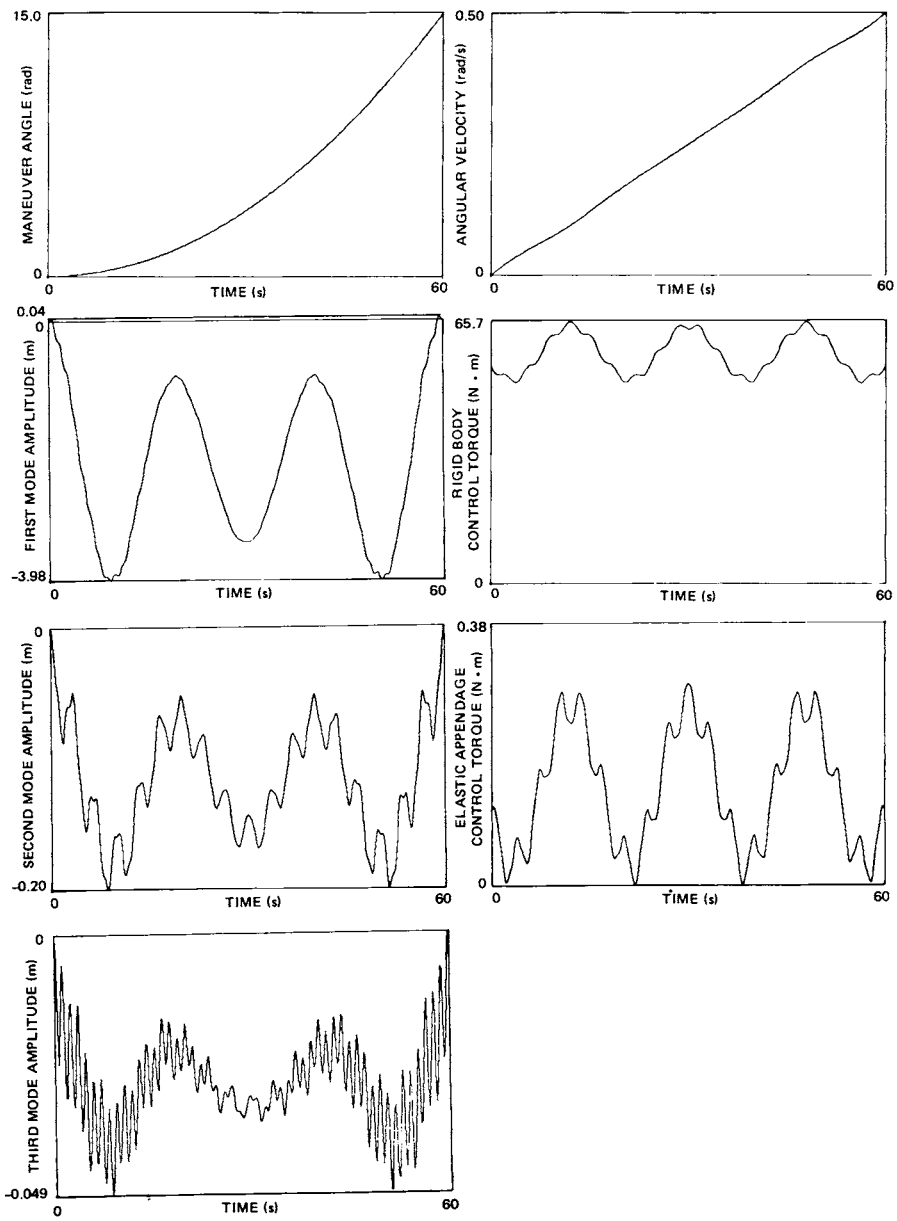

Figure 9.9 Case 7, Linear Free Final Angle Spinup Maneuver, 3 Modes, 5 Controls

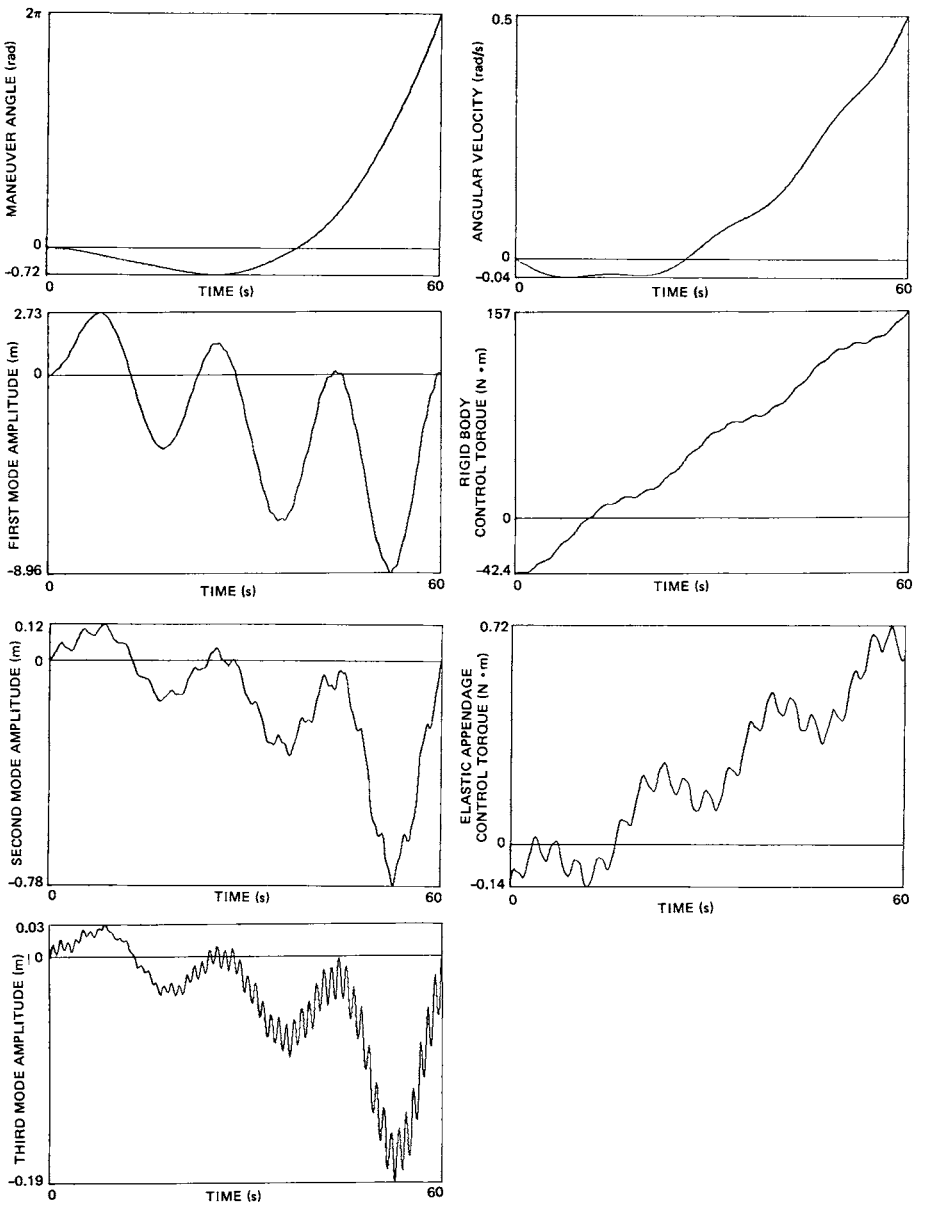

Figure 9.10 Case 8, Nonlinear Spinup Maneuver, 3 Modes, 5 Controls

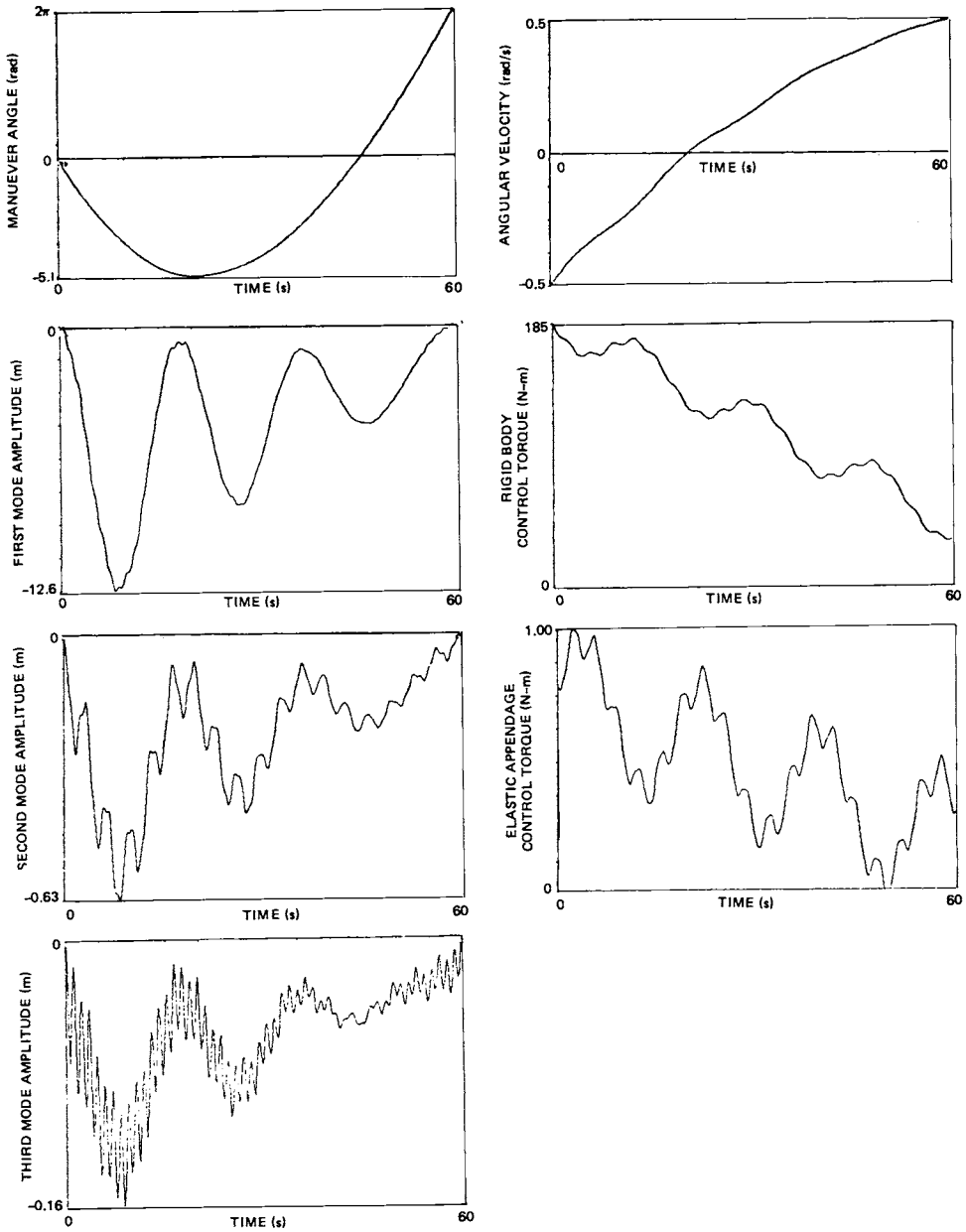

Figure 9.11 Case 9, Rotation Reversal, Linear Kinematics, 3 Modes, 5 Controls

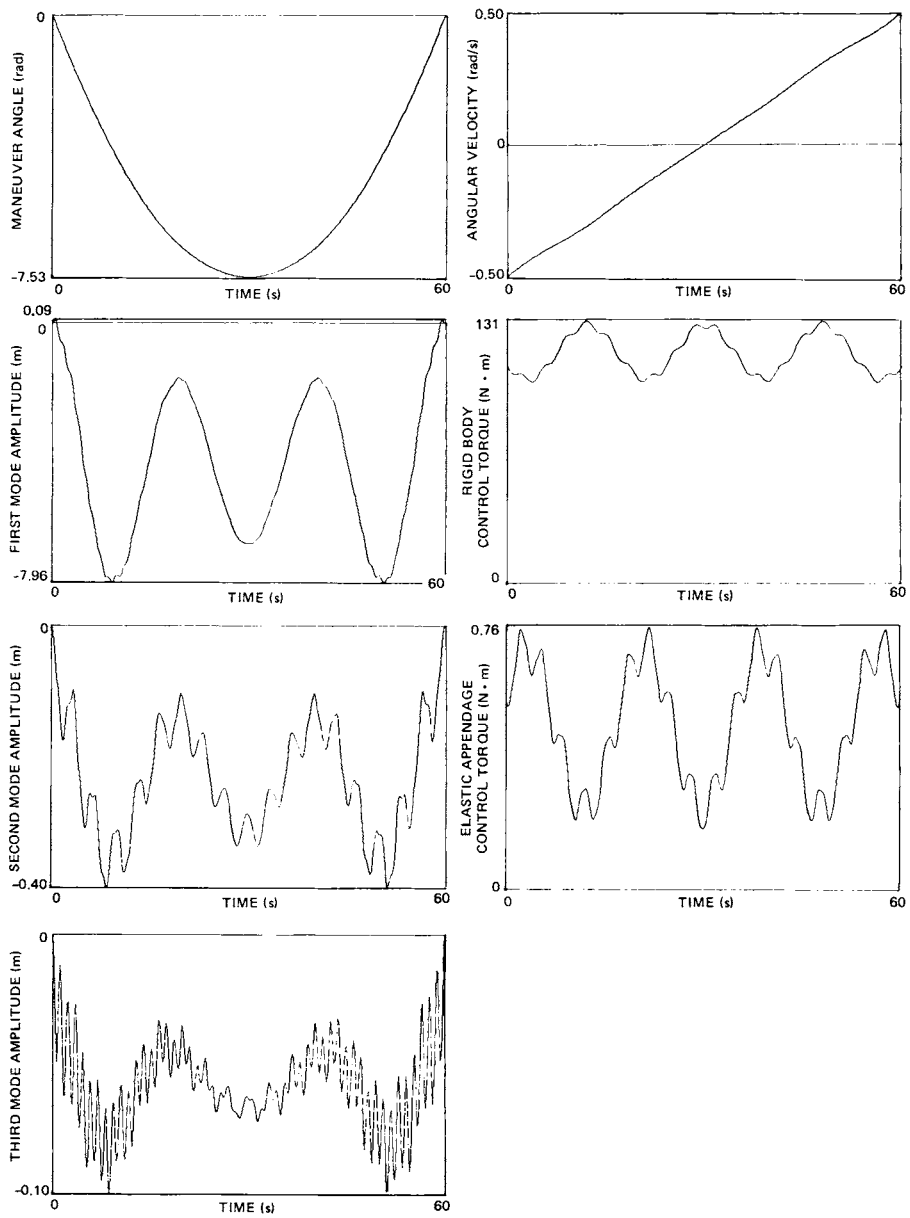

Figure 9.12 Case 10, Linear Free Final Angle Spin Reversal Maneuver, 3 Modes, 5 Controls

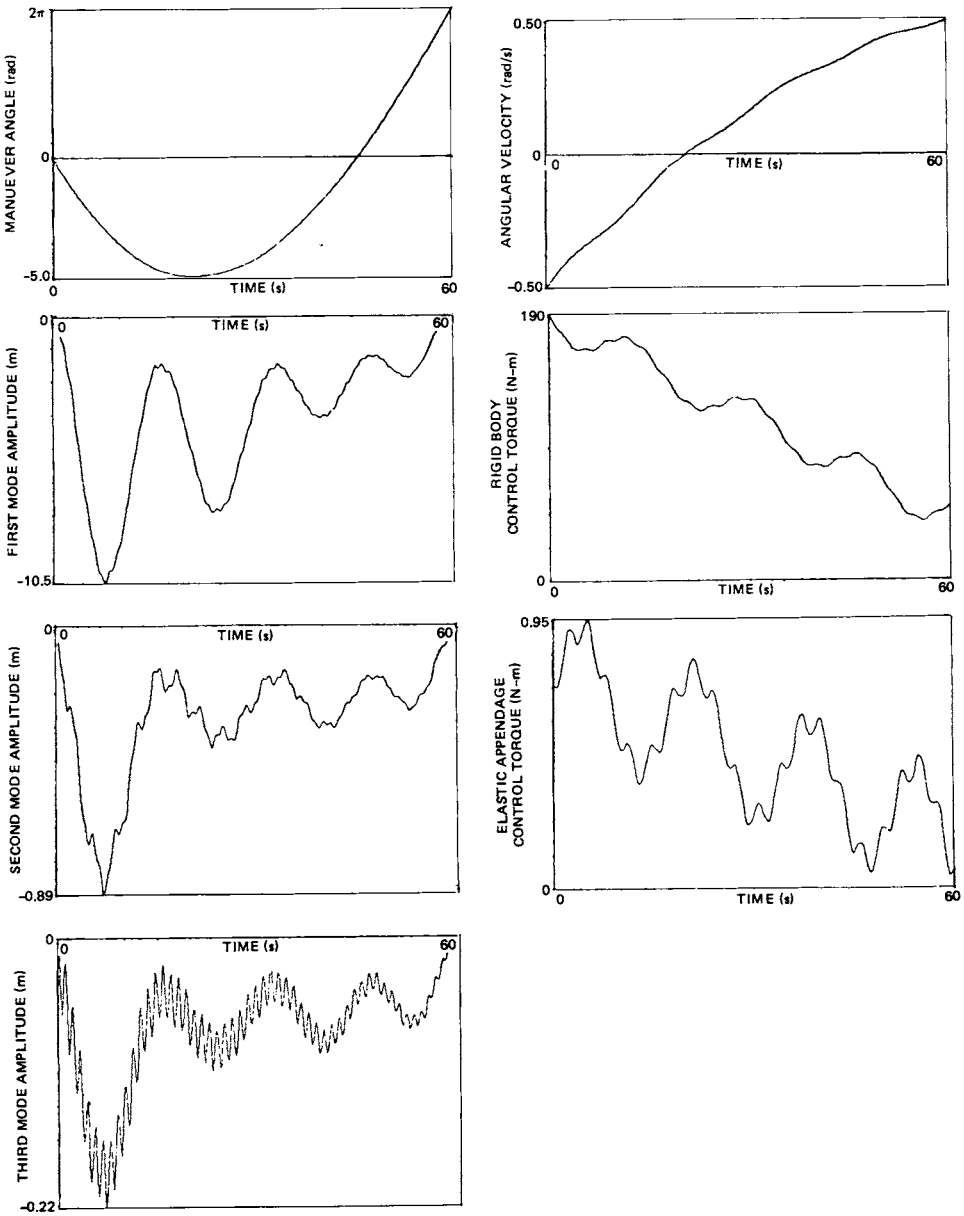

Figure 9.13 Case 11, Rotation Reversal, Nonlinear Kinematics, 3 Modes, 5 Controls

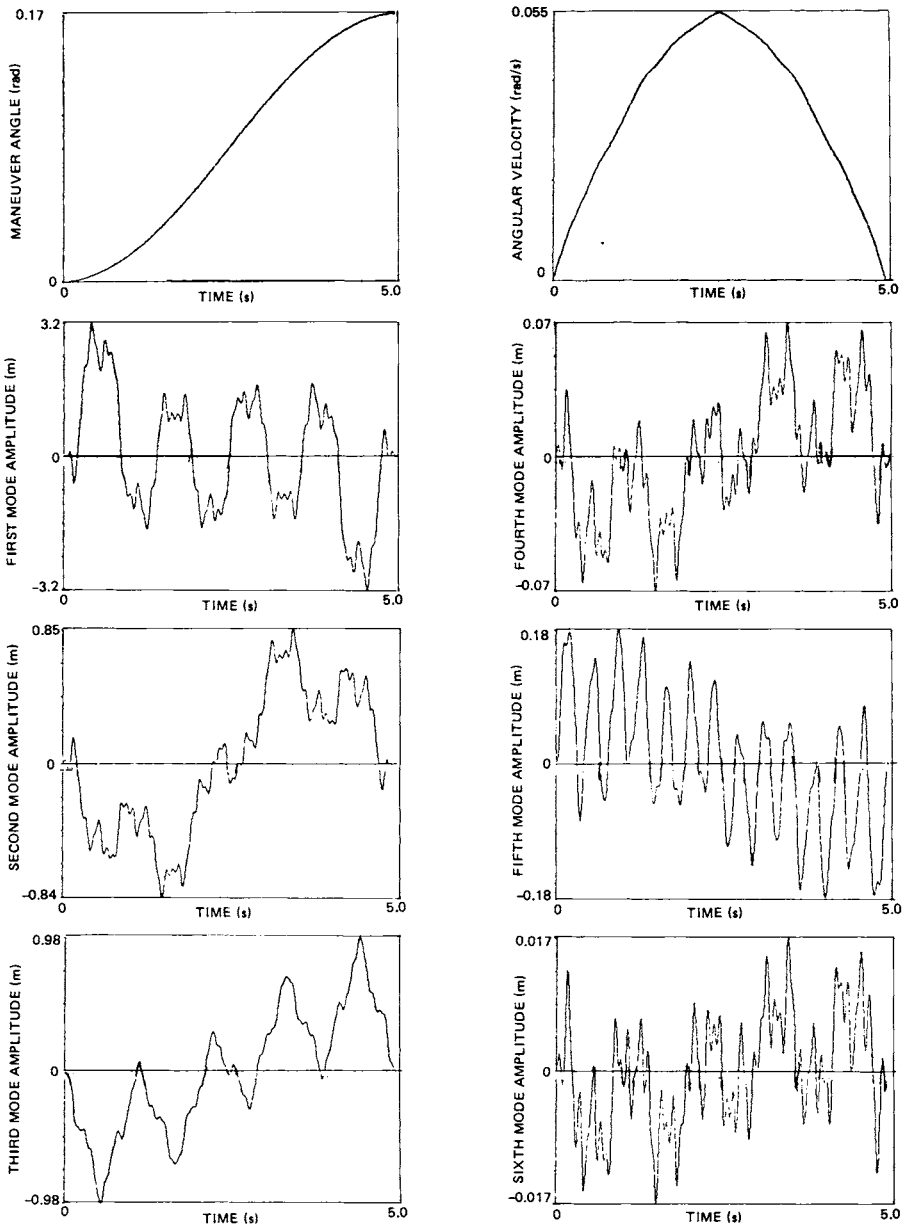

Figure 9.14a Case 12, 10-Modes, Rest-to-Rest Maneuver

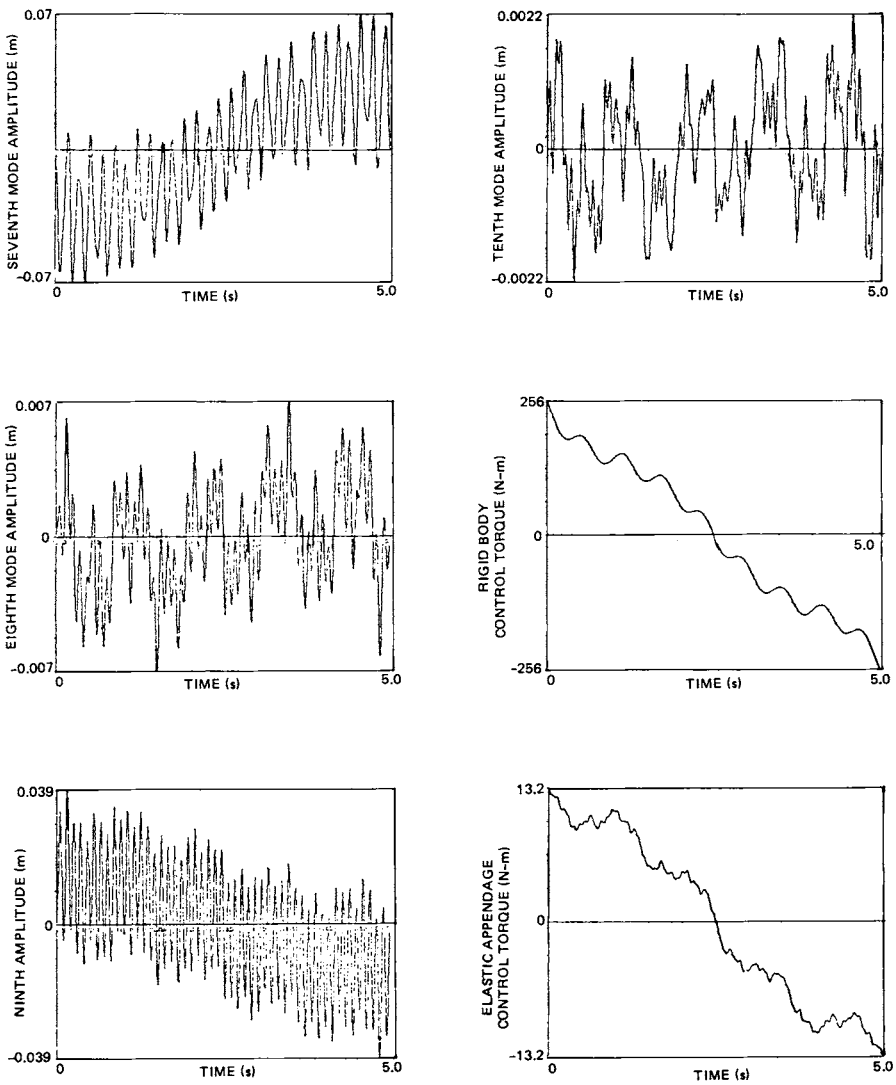

Figure 9.14b Case 12, 10-Modes, Rest-to-Rest Maneuver (cont.)

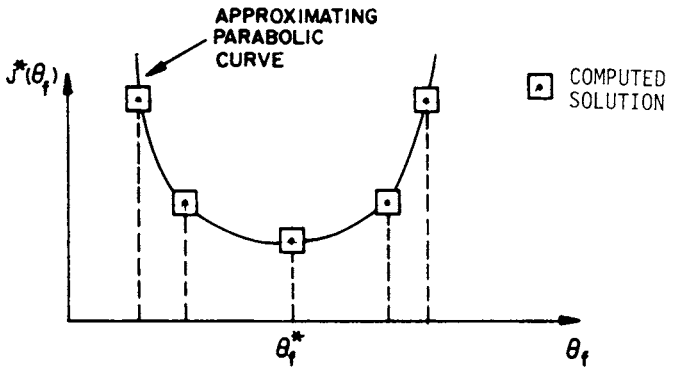

Figure 9.15 Performance Versus Final Angle

(3) As the number of modes retained in the dynamical model increases, the state weighting must decrease; in order to maintain a fixed eigenvalue bandwidth for the state/co-state system. This result is important; since the product of the maneuver time and the state/co-state eigenvalue bandwidth has an upper limit, for which the optimal control problem can be reliably solved using numerical methods;

(4) For maneuvers where the final angular rate (and not the final attitude angle) is important, the optimal solution is improved by allowing the control algorithm to select the *natural boundary condition* for terminal rigid body angle, leading to improved system performance as measured by:

(a) reduced peak flexural deflections;

(b) reduced peak torque requirements; and

(c) minimum performance index cost as measured as a function of the final maneuver angle (see Figure 9.15);

(5) Nonlinear effects do not usually influence the vehicle's response significantly unless high angular rates are achieved during the maneuver. In fact, it has been shown that high rotation rates usually leads to decreased peak structural deflections when one accounts for the stiffening effect;

(6) The optimal control time histories of the present chapter have jump discontinuities initially and finally; and

(7) The use of a distributed set of discrete controllers significantly improves the system performance. However, once each elastic appendage has one controller, when additional controllers are added the gain in the system performance is marginal.

As shown in Figure 9.15, when the performance index $J^*(\theta_f)$ is plotted as a function of the final maneuver angle θ_f (where the maneuver time, weighting matrices, and boundary conditions other than θ_f are held fixed), we find that the sequence of optimal performance indices, has a minimum at the final angle determined by the free final angle transversality condition. From Figure 9.10 we see that the free final angle transversality condition yields a *natural boundary condition* for the maneuver. In Chapter 6, Figure 6.13, we note that the performance index for the rigid body case behaves identically and is rigorously a quadratic function of θ_f. Of course, other parameters in the problem formulation can be allowed to go free, such as the final time. However, the special needs of particular maneuvers will usually dictate the various boundary condition formulations, as well as suggest alternative performance indices and associated weight matrices.

In Chapter 10, the optimal control generalizations necessary to extend the results of this chapter to the case where the terminal control on/off jump discontinuities are eliminated and smoother torque histories are obtained.

REFERENCES

1. Meirovitch, L., **Methods of Analytical Dynamics**, McGraw-Hill Book Co., New York, 1970, p. 68.

2. Meirovitch, L., "A Stationary Principle for the Eigenvalue Problem for Rotating Structures," **AIAA Journal**, Vol. 14, Oct., 1976, pp. 1387-1394.

3. Bryson, A. E., and Y. C. Ho., **Applied Optimal Control**, John Wiley & Sons, Inc., New York, 1975, Chapters 2 and 5.

4. Young, Y. C., **Calculus of Variations and Optimal Control Theory**, W. B. Saunders, Co., Philadelphia, PA, pp. 308-321.

5. Leitmann, G., **Optimization Techniques with Applications to Aerospace Systems**, Academic Press, New York, 1962, Chapter 7, (R. E. Kopp's contribution).

6. Pontryagin, L. S., et al., **The Mathematical Theory of Optimal Processes**, Interscience, London, 1962.

7. Kirk, D. E., **Optimal Control Theory. An Introduction**, Prentice Hall, New Jersey, 1970.

8. Moler, C., and C. V. Loan, "Nineteen Dubious Ways to Compute the Exponential of a Matrix," **SIAM Review**, Vol. 20, No. 4, Oct. 1978.

9. Ward, R. C., "Numerical Computation of the Matrix Exponential with Accuracy Estimate," **SIAM J. Numer. Anal.**, Vol. 14, No. 4, Sept. 1977.

10. Turner, J. D., "Optimal Large-Angle Spacecraft Rotational Maneuvers," Ph.D. Dissertation, Virginia Polytechnic Institute and State University, Blacksburg, VA, 1980.

11. Chun, H. M., "Optimal Distributed Control of a Flexible Spacecraft During a Large-Angle Rotational Maneuver," Master's Thesis, Massachusetts Institute of Technology, Cambridge, MA, June 1982.

12. Dennis, J. E., Jr., and R. B. Schnabel, "Least Change Secant Updates for Quasi-Newton Methods," **SIAM Review**, Vol. 21, No. 4, pp. 443-459, Oct. 1979.

13. Greenstadt, J., "Variations on Variable-Metric Methods," **Mathematics of Computation**, Vol. 24, No. 109, pp. 1-22, Jan. 1970.

14. Goldfarb, D., "A Family of Variable-Metric Methods Derived by Variational Means," **Mathematics of Computation**, Vol. 24, No. 109, pp. 23-26, Jan. 1970.

15. Schmidt, W. F., "Adaptive Step Size Selection for Use with the Continuation Method," **International Journal for Numerical Methods in Engineering**, Vol. 12, pp. 677-694, 1978.

16. Deuflhard, P., H. J. Resch, and P. Rentrap, "A Modified Continuation Method for the Numerical Solution of Nonlinear Two-Point Boundary-Value Problems by Shooting Techniques", **Numer. Math.**, Vol. 26, pp. 327-343, 1976.

17. Junkins, J. L., and Turner, J. D., "Optimal Continuous Torque Attitude Maneuvers," **Journal of Guidance and Control**, Vol. 3, No. 3, May-June 1980, pp. 210-217.

18. Roberts, S. M., Shipman, J. S., Roth, C. V., "Continuation in Quasilinearization, **J. of Optimization Theory and Appl.**, Vol. 2, No. 3 (1968), 164-178.

19. Chow, S. N., Mallet-Paret, J., and Yorke, J. A., "Finding Zeros of Maps: Homotopy Methods that are Constructive with Probability One," **Math. Comp.**, Vol. 32, 1978, pp. 887-889.

20. Watson, L. T., "A Globally Convergent Algorithm for Computing Fixed Points of C^2 Maps," **APP. Math. Comput.**, Vol. 5, 1979, pp. 297-311.

21. Watson, L. T., and Fenner, D., "Chow-Yorke Algorithms for Fixed Points or Zeros of C^2 Maps," **ACM Trans. Math. Software**, Vol. 6, 1980, pp. 252-260.

22. Dunyak, J. P., Junkins, J. L., and Watson, L. T., "Robust Nonlinear Least Squares Estimation Using the Chow-Yorke Homotopy Method," **AIAA J. of Guidance, Control and Dynamics**, Vol. 7, No. 4, July, August 1984, pp.

23. Turner, J. D. and Chun, H. M., "Optimal Distributed Control of a Flexible Spacecraft During a Large-Angle Rotational Maneuver," **Journal of Guidance, Control, and Dynamics**, Vol. 7, No. 3, May-June, 1984, pp. 257-264.

24. Junkins, J. L., Bodden, D. S., and Turner, J. D., "A Unified Approach to Structure and Control System Iterations," Proceedings of **The 4th International Conference on Applied Numerical Modeling**, Tainan, Taiwan, December, 1984.